Global Teleconnections of Meridional Overturning Circulation Anomalies

HELEN L. JOHNSON* AND DAVID P. MARSHALL

Department of Meteorology, University of Reading, Reading, United Kingdom

(Manuscript received 6 January 2003, in final form 15 December 2003)

ABSTRACT

There is a wide range of evidence from both models and palaeoclimatic data that indicates the possibility of abrupt changes in the oceanic meridional overturning circulation (MOC). However, much of our dynamical understanding of the MOC comes from steady-state models that rely upon the assumption of thermodynamic equilibrium and are therefore only valid on millennial time scales. Here a dynamical model for the global teleconnections of MOC anomalies on annual to multidecadal time scales is developed. It is based on a linear theory for the propagation of zonally integrated meridional transport anomalies in a reduced-gravity ocean and allows for multiple ocean basins connected by a circumpolar channel to the south. The theory demonstrates that the equator acts as a low-pass filter to MOC anomalies. As a consequence, MOC anomalies on decadal and shorter time scales are confined to the hemispheric basin in which they are generated and have little impact on the remainder of the global ocean. The linear theory is compared with the results of a global nonlinear numerical integration, which it reproduces to a good approximation.

1. Introduction

State-of-the-art climate models suggest that the meridional overturning circulation (MOC) in the Atlantic Ocean is likely to weaken over the next century, although there is little consensus on the rate and magnitude of the likely changes (Houghton et al. 2001). Moreover, there is evidence from a range of models to suggest that the MOC might possess more than one stable mode of operation and is liable to collapse in a warming climate (e.g., Stommel 1961; Marotzke and Willebrand 1991; Manabe and Stouffer 1994). Abrupt changes between different MOC states are also suggested by a number of palaeoclimate records (e.g., Broecker and Denton 1989).

Despite the distinct possibility of abrupt changes, much of our dynamical understanding of the MOC is based on steady-state theory, as initiated by Stommel and Arons (1960), Stommel (1961), and Munk (1966). However, steady-state theories for the MOC assume thermodynamic equilibrium, which occurs only on millenial time scales, whereas rapid changes in MOC can occur over much shorter periods. The ocean is forced by the atmosphere on all time scales, with wind forcing dominating MOC variability on interannual and shorter time scales (Dong and Sutton 2001), but with buoyancy forcing perhaps dominating on decadal time scales (Häkkinen 2001; Eden and Willebrand 2001). To monitor changes in the MOC successfully and to attribute these changes to thermohaline forcing at high latitudes, we need to understand the causes, propagation, and attenuation of MOC anomalies on all time scales.

In this paper, we develop a theoretical model for the global propagation of MOC anomalies forced on annual to multidecadal time scales. Numerical experiments using general circulation models have made progress on understanding the response of the MOC to changes in surface forcing, both realistic [e.g., Eden and Jung (2001) and Eden and Willebrand (2001), who consider the response in the North Atlantic to more than 100 years of forcing associated with the North Atlantic Oscillation] and idealized (e.g., Goodman 2001). Others have taken a theoretical approach in establishing the localized response of the ocean to periodic wind and buoyancy forcing (e.g., Liu 1993; Liu and Pedlosky 1994), and Karcher (1997) has considered the response of an abyssal reduced-gravity layer in a North Atlantic domain to periodic high-latitude forcing.

The model developed here builds on that described in Johnson and Marshall (2002a,b) in which a reduced-gravity isopycnal layer (representing the surface limb of the MOC) is forced by a prescribed mass source or sink at high latitudes (representing the formation of deep water). Because the vertical structure of the MOC is dominated by the first baroclinic mode, with a single reversal at the approximate depth of the thermocline,

* Current affiliation: School of Earth and Ocean Sciences, University of Victoria, Victoria, British Columbia, Canada.

Corresponding author address: Helen L. Johnson, School of Earth and Ocean Sciences, University of Victoria, P.O. Box 3055, Victoria, BC V8W 3P6, Canada.
E-mail: helenj@uvic.ca

we might expect a reduced-gravity model to provide a useful zero-order description [see Wajsowicz (1986) for a comparison with the response of a general circulation model]. In the absence of variations in bottom topography and background mean flow, the theory developed here can be easily extended to a continuously stratified ocean by projecting onto the spectrum of baroclinic modes.

As found by Wajsowicz and Gill (1986) and Kawase (1987), the initial dynamical adjustment to changes in high-latitude forcing is through the propagation of Kelvin waves around the perimeter of the basin, on time scales of a few months, followed by the radiation of Rossby waves off the eastern boundary into the ocean interior, on time scales of a few months at low latitudes to several years at high latitudes. The same adjustment process has been observed in a wide hierarchy of models (e.g., Döscher et al. 1994; Karcher and Lippert 1994; Greatbatch and Peterson 1996; Winton 1996; Yang 1999; Goodman 2001; Dong and Sutton 2002). Although some models suggest that the advection of deep density anomalies may also be important [e.g., Gerdes and Köberle (1995), who see a two-stage adjustment that consists of a baroclinic-wave response followed by an advective response, Marotzke and Klinger (2000), and Goodman (2001)], the choice of a reduced-gravity framework here restricts our focus to the surface adjustment processes, which are the most likely to feed back on the atmosphere on the decadal to multidecadal time scales of interest.

The crucial ingredient emphasized by Johnson and Marshall (2002a) is the role of the equator. In specific terms, they note that the amplitude of the boundary pressure anomaly within a western boundary Kelvin wave is greatly reduced by the time the Kelvin wave reaches the equator; this pressure anomaly is not reamplified when the Kelvin wave subsequently returns poleward along the eastern margin of the basin. As a consequence, the pressure anomaly radiated westward into the basin interior by Rossby waves represents only a small fraction of the original high-latitude forcing. Johnson and Marshall (2002a) term this mechanism the "equatorial buffer" because it restricts the amplitude of the response in the unforced hemisphere on short time scales. As a result of this buffering mechanism, the equator acts as a low-pass filter to MOC anomalies (Johnson and Marshall 2002b; Liu et al. 1999).

By relating the zonal propagation of layer thickness anomalies (by Rossby waves) to the divergence of the MOC, Johnson and Marshall (2002a) derive an equation for the adjustment of the layer thickness on the eastern boundary, from which the adjustment of the MOC can be deduced. Results of this single-parameter theoretical model agree extremely favorably with the results of full numerical calculations (Johnson and Marshall 2002a,b). The mathematics of this MOC adjustment problem are similar to the mathematics of the damped "basin modes" discussed by LaCasce (2000), Cessi and Primeau (2001), Cessi and Paparella (2001), Cessi and Louazel (2001), Liu (2002), and Primeau (2002). However, the forcing is applied at the western boundary in the present problem, rather than in the basin interior, and, as a result, the resonance of the basin modes at decadal frequencies turns out to be weak.

Primeau (2002) and Cessi and Otheguy (2003) have recently questioned the relevance of Kelvin waves to the ocean's adjustment on decadal and multidecadal time scales. Both point out that the wavelength of a Kelvin wave forced at such low frequencies will greatly exceed the length of the coastline around which it travels. We do not view these long wavelengths as a problem, since there is no requirement for an integral number of wavelengths to fit within the basin. Because the theory developed here depends only on the existence of some form of boundary adjustment process that acts to make pressure uniform on the eastern boundary on time scales longer than a few months, the role of Kelvin waves specifically is not critical to our results. In the real ocean, where the boundary consists of a sloping bottom, the signal is more likely to propagate as a coastally trapped topographic wave on the continental shelf. We use the term Kelvin wave throughout to describe the propagation of a coastally trapped thickness anomaly at approximately the gravity-wave speed, and it is left to the reader to make up his or her own mind on the matter.

The remainder of the paper is structured as follows. In section 2 we extend the theory derived in Johnson and Marshall (2002a) to obtain an expression for the amplitude of MOC anomalies in an idealized rectangular basin as a function of latitude and frequency. In section 3 the theory is then further extended to multiple connected ocean basins. In section 4, we apply the model to a realistic global ocean geometry, and the theory is validated through comparison with the results of a full numerical calculation. A concluding discussion in given in section 5.

2. Theory for a single basin

We first consider the response of a single reduced-gravity basin to a periodic forcing at its high-latitude margin. Preliminary calculations employing a realistic Atlantic domain were reported in Johnson and Marshall (2002b). Here we develop the underlying theory for the propagation of MOC anomalies in a single basin.

a. *Model formulation*

Following Johnson and Marshall (2002a), we consider an idealized, reduced-gravity ocean basin that spans the equator and is open to the south. The model is intended to represent the warm, upper limb of the MOC in the Atlantic. Flow is forced on the northern boundary by a prescribed northward transport T_N that represents the net conversion of surface water into deep water at high latitudes. (Equivalently, one can specify the layer thickness in the northwest corner of the domain to parameterize the effects of deep convection, and this leads to identical results.) At the southern boundary, a northward transport T_S is allowed to represent the flow of water into the Atlantic from the remaining basins (details of how T_S is prescribed are given below).

Under the assumptions of geostrophic balance and a linearized continuity equation in the interior, the adiabatic response of a reduced-gravity model is described by the mass budget equation derived in Johnson and Marshall (2002a):

$$T_N - T_S = \int_{\phi_S}^{\phi_N} Rc[h_e(t - L/c) - h_e(t)]\, d\phi, \tag{1}$$

where $R = 6.373 \times 10^6$ m is the radius of the earth, h_e is the surface-layer thickness on the eastern boundary, $L(\phi)$ is the width of the basin, t is time,

$$c = \frac{\beta g' H}{f^2} = \frac{g' H \cos\phi}{2\Omega R \sin^2\phi} \tag{2}$$

is the Rossby wave speed, β is the meridional gradient of the Coriolis parameter f, g' is the reduced gravity, H is the initial surface-layer thickness, and $\Omega = 7.29 \times 10^{-5}\ \mathrm{s}^{-1}$ is the rotation rate of the earth.

This equation is based on a time scale separation between the fast boundary/equatorial Kelvin waves and the much slower Rossby wave adjustment in the interior. It assumes that the Kelvin wave speed is infinite such that the surface layer thickness along the eastern boundary and the equator is uniform at any given time. In physical terms, Eq. (1) expresses the fact that the divergence in meridional transport ($T_N - T_S$) is determined by the difference between the surface-layer thickness anomaly communicated by Rossby waves into the western boundary current $[h_e(t - L/c)]$ and that propagated into the interior on the eastern side of the basin $[h_e(t)]$, integrated over the entire meridional extent of the domain.

On the southern boundary, the transport T_S is determined by integrating geostrophic balance across the basin and linearizing to give

$$T_S = \frac{g' H}{f_S}(h_e - h_{\mathrm{SW}}), \tag{3}$$

where the layer thickness in the southwest corner of the domain h_{SW} is equal to the constant H. This boundary condition is based on the assumption that the layer thickness in the southwest corner of the Atlantic is set by Kelvin waves propagating around the southern tip of South America from the Pacific; we will see in sections 3 and 4 that setting h_{SW} equal to a constant is justified on time scales shorter than a few decades.

Given a prescribed forcing on the northern boundary T_N, Eq. (1) can be used to predict the time-dependent adjustment of the system.

b. Theory for periodic forcing

If the forcing is periodic, with a solution of the form $e^{i\omega t}$, then

$$h_e = h_0 + Ae^{i\omega t}, \quad \text{and} \tag{4}$$

$$T_N = T_0 e^{i\omega t}, \tag{5}$$

where A is the amplitude of variability in layer thickness on the eastern boundary. After dividing through by $e^{i\omega t}$, Eq. (1) becomes

$$T_0 = A\left\{\frac{g' H}{f_S} - \int_{\phi_S}^{\phi_N} Rc[1 - e^{(-i\omega L)/c}]\, d\phi\right\}, \tag{6}$$

from which one can determine A.

A mass budget equation similar to Eq. (1) can also be derived over a limited latitudinal range. Integrating from the southern boundary to a latitude ϕ gives the zonally integrated transport $T(\phi, \omega)$ as a function of latitude and frequency:

$$T(\phi, \omega) - T_S = \int_{\phi_S}^{\phi} Rc[h_e(t - L/c) - h_e(t)]\, d\phi, \tag{7}$$

which, after substitution, results in

$$T(\phi, \omega) = Ae^{i\omega t}\left\{\frac{g' H}{f_S} - \int_{\phi_S}^{\phi} Rc[1 - e^{(-i\omega L)/c}]\, d\phi\right\}. \tag{8}$$

Dividing Eq. (8) by T_N and substituting for T_0 using Eq. (6) results in an expression for the reduction in amplitude of the meridional transport anomaly in the upper layer as a function of latitude and frequency:

$$\frac{T}{T_N}(\phi, \omega) = \frac{\dfrac{g' H}{f_S} - \displaystyle\int_{\phi_S}^{\phi} Rc[1 - e^{(-i\omega L)/c}]\, d\phi}{\dfrac{g' H}{f_S} - \displaystyle\int_{\phi_S}^{\phi_N} Rc[1 - e^{(-i\omega L)/c}]\, d\phi}. \tag{9}$$

Equation (9) is a complex fraction whose modulus $|T/T_N|$ gives the amplitude of the variability in zonally integrated meridional volume transport at each latitude, as a fraction of the prescribed variability on the northern boundary. The argument of Eq. (9) gives the phase lag. Note that the numerator and denominator only differ in the latitudinal extents over which the integral is evaluated.

c. Results

Figure 1 shows the numerical solution of Eq. (9) for an idealized sector ocean basin 50° wide, where $L = L_0 \cos\phi$, $L_0 = 5.5 \times 10^6$ m, $g' = 0.02\ \mathrm{m\ s^{-2}}$, $H = 500$ m, $\phi_S = 36°$S, and $\phi_N = 65°$N. Figure 1a shows the modulus $|T/T_N|$, which gives the amplitude of the variability in meridional transport at each latitude as a fraction of the amplitude of the forcing on the northern boundary.

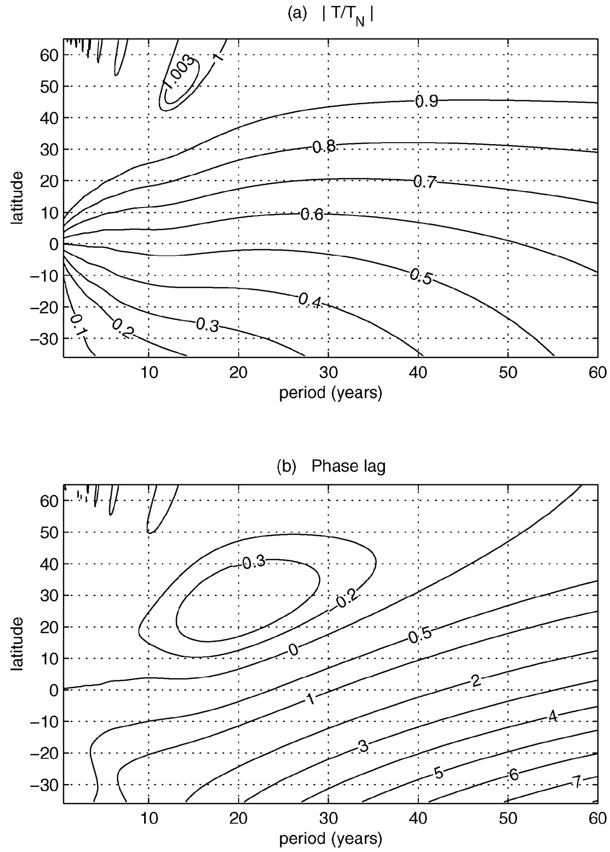

FIG. 1. Numerical solution of Eq. (9) for an idealized sector ocean basin. (a) Modulus $|T/T_N|$, which gives the amplitude of the variability in meridional transport as a fraction of the prescribed variability on the northern boundary. (b) Phase lag $\arg(T/T_N)$ of the variability behind the forcing, in years.

At decadal frequencies and higher, the amplitude is approximately constant throughout most of the Northern Hemisphere but is greatly reduced in the Tropics. The signal in the Southern Hemisphere is small. As the frequency of the forcing decreases, the region over which the amplitude reduction occurs becomes broader such that at multidecadal frequencies the amplitude of the variability decreases throughout the entire domain. At these lower frequencies much more of the variability is transmitted to the southern boundary. For a forcing period of 50 yr, 50% of the signal reaches 30°S.

For variability with a period of about 13 yr, the amplitude of the response at high latitudes in the North Atlantic is slightly *larger* than that of the forcing. This is the result of a weak resonance of the basin modes described by LaCasce (2000), Cessi and Primeau (2001), Cessi and Paparella (2001), Cessi and Louazel (2001), Liu (2002), and Primeau (2002). The period of these oscillatory modes is controlled by the time taken for a Rossby wave to cross the basin at its northern margin:

$$t(\phi) = \frac{2\Omega R L_0}{g' H} \sin^2\phi_N. \tag{10}$$

At the northernmost extent of our model (65°N), this Rossby wave transit time is 13.3 yr. If the forcing on the northern boundary has a period of 13.3 yr, then the signal returning via the westward-propagating Rossby wave will be in phase with the forcing and will amplify it, leading to a resonance effect. This condition will also occur at all harmonics of the resonant frequency (corresponding to periods of 6.6 yr, 3.3 yr, etc.) and is clear in Fig. 1a.

The basin modes are only weakly excited because, unlike in previous studies that have been forced largely by wind and buoyancy anomalies within the ocean interior, here the forcing is applied exclusively at the western boundary. The resultant boundary pressure anomaly is heavily damped as the Kelvin wave propagates equatorward along the western boundary and does not reamplify as the Kelvin wave returns poleward along the eastern boundary (Johnson and Marshall 2002a). As a consequence the forcing ''seen'' by the ocean interior, which can in turn resonate a basin mode, is only a small fraction of that originally applied at the western boundary.

Figure 1b shows the phase lag, in years, of the variability at each latitude in comparison with the forcing. Variability with a period of less than 20 yr is transmitted with almost no lag to the equator (there is, in fact, a small phase *lead*, presumably due to interference effects). South of the equator, the phase lag increases with latitude. For multidecadal variability both the Northern and Southern Hemispheres experience a phase lag that decreases with frequency and increases with distance from the forcing region such that, on the southern boundary, variability with a period of 50 yr lags behind the forcing by about 7 yr. In the low-frequency limit, the phase lag varies approximately linearly with latitude and is independent of frequency. (The phase lag in Fig. 1 should be viewed in the light of the amplitude reduction illustrated in the upper panel; at high frequency, signals in the Southern Hemisphere are so small that the phase lag is meaningless.)

Figure 1a shows that the spatial extent of variability is highly dependent on frequency. The equator acts as a low-pass filter, restricting decadal and higher-frequency variability to the hemisphere in which it is generated. This low-pass filtering results from the difference, outlined in Johnson and Marshall (2002a,b), in the mechanism by which overturning anomalies propagate southward in each hemisphere. High-latitude variability is transmitted efficiently throughout the entire hemisphere in which it is forced by fast Kelvin waves that propagate along the western boundary to the equator (Kawase 1987). In the opposite hemisphere, however, a fast response on the western boundary is not possible, and eastern boundary Kelvin waves are inefficient at communicating overturning anomalies poleward (because they radiate Rossby waves that propagate westward into the interior). As a consequence of its slower adjustment, the second hemisphere cannot respond to high-frequency variability before the forcing changes sign. Only variability on decadal time scales and longer has a significant influence.

Low-pass filtering by the Tropics was demonstrated in a realistic Atlantic-shaped domain using a fully nonlinear numerical reduced-gravity model in Johnson and Marshall (2002b). Agreement between the theory and the numerical calculation is good in both idealized (not shown) and realistic domain geometries, suggesting that the theory successfully captures the response of the model's Atlantic overturning circulation to variability in forcing at high latitudes.

3. Two basins

In the previous section, discussion of the spatial extent of variability was limited to the Atlantic sector. Here the effect of thermohaline overturning anomalies in the high-latitude North Atlantic on the rest of the global ocean is considered. The theory will be built up in stages, beginning with the case of two idealized sector ocean basins. A realistic global ocean geometry will be considered subsequently in section 4.

To solve for a single basin, it is necessary to prescribe the surface-layer thickness in the southwest corner of the domain h_{SW} [see Eq. (3)]. So far the value of h_{SW} has been assumed to be constant and equal to the initial surface-layer thickness H (and hence to h_0). In reality it will be set by Kelvin waves propagating around the southern tip of South America from the Pacific Ocean. The linearized southern boundary condition then becomes

$$T_S = \frac{g'H}{f_S}(h_A - h_P), \tag{11}$$

where h_A is the surface-layer thickness on the eastern boundary of the Atlantic and h_P is the surface-layer thickness on the eastern boundary of the Pacific. In this way the adjustment between basins is coupled through the geostrophic flow across their southern boundaries.

Consider first the simplified case of two identical sector ocean basins, separated by continental land masses that extend to the same latitude ϕ_S, south of the equator, and connected through a zonal channel to the south (see Fig. 2). Variable thermohaline forcing $T_N = T_0e^{i\omega t}$ is applied to the northern boundary of basin 1, and there is a closed northern boundary in basin 2. The applied forcing has a mean of zero so that there is no net gain or loss of mass from the surface layer—the ocean adjustment is assumed to be entirely adiabatic on the decadal and multidecadal time scales of interest here. Layer thickness in the southwest corner of each basin is set by Kelvin waves propagating along the coast from the basin immediately to the west.

Proceeding as in section 2, the mass budget equation for basin 1 can be expressed as

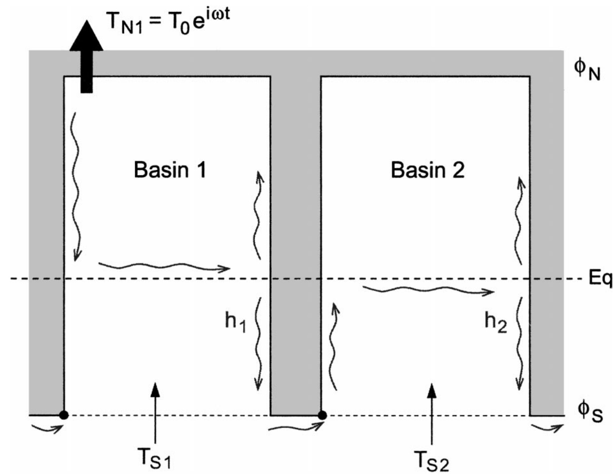

FIG. 2. Schematic illustrating two identical sector ocean basins, each extending from ϕ_S to ϕ_N, and connected by a zonal channel to the south. Thickness anomalies are transmitted from one basin to the next by Kelvin waves, which propagate in the direction shown. A linear, geostrophic boundary condition is applied to the south of each basin (straight arrows) such that flow leaving basin 1 is assumed to enter basin 2.

$$\frac{\partial}{\partial\phi}T_1(\phi, t) = Rc\left[h_1\left(t - \frac{L_1}{c}\right) - h_1(t)\right], \tag{12}$$

where

$$h_1 = h_0 + A_1e^{i\omega t},$$
$$T_{N1} = T_0e^{i\omega t},$$
$$T_{S1} = \frac{g'H}{f_S}(h_1 - h_2),$$

h_1 is the surface-layer thickness (h_e) on the eastern boundary of basin 1, and h_2 is the equivalent in basin 2. For basin 2,

$$\frac{\partial}{\partial\phi}T_2(\phi, t) = Rc\left[h_2\left(t - \frac{L_2}{c}\right) - h_2(t)\right], \tag{13}$$

$$h_2 = h_0 + A_2e^{i\omega t},$$
$$T_{N2} = 0, \quad \text{and}$$
$$T_{S2} = \frac{g'H}{f_S}(h_2 - h_1).$$

Note that $T_{S1} = -T_{S2}$, reflecting the fact that flow leaving basin 1 at its southern boundary is assumed to enter basin 2. There is no net flow into or out of the domain apart from the prescribed forcing T_{N1}.

Integrating Eqs. (12) and (13) over the entire meridional extent of the domain and dividing through by $e^{i\omega t}$ leads to

$$T_0 - \frac{g'H}{f_S}(A_1 - A_2) + A_1 \int_{\phi_S}^{\phi_N} Rc[1 - e^{(-i\omega L_1)/c}]\, d\phi = 0 \quad \text{and} \tag{14}$$

$$-\frac{g'H}{f_S}(A_2 - A_1) + A_2 \int_{\phi_S}^{\phi_N} Rc[1 - e^{(-i\omega L_2)/c}]\, d\phi = 0. \tag{15}$$

Integrating the same two equations from the southern extent of each basin up to a latitude ϕ gives

$$T_1(\phi, \omega) = e^{i\omega t}\left\{\frac{g'H}{f_S}(A_1 - A_2) - A_1 \int_{\phi_S}^{\phi} Rc[1 - e^{(-i\omega L_1)/c}]\, d\phi\right\} \tag{16}$$

and

$$T_2(\phi, \omega) = e^{i\omega t}\left\{\frac{g'H}{f_S}(A_2 - A_1) - A_2 \int_{\phi_S}^{\phi} Rc[1 - e^{(-i\omega L_2)/c}]\, d\phi\right\}. \tag{17}$$

Here A_1 and A_2 are the amplitudes of the variability in layer thickness on the eastern boundaries of basins 1 and 2, respectively.

a. Basin factor

Equation (15) can be rearranged to give

$$\frac{A_2}{A_1} = \frac{\dfrac{g'H}{f_S}}{\dfrac{g'H}{f_S} - \displaystyle\int_{\phi_S}^{\phi_N} Rc[1 - e^{(-i\omega L_2)/c}]\, d\phi}. \tag{18}$$

This "basin factor" is the ratio of the surface-layer thickness anomalies on the eastern boundaries of basin 2 and basin 1. It varies with frequency and depends upon the geometry of basin 2 (but not of basin 1). All that is required to calculate this ratio for any pair of ocean basins is the width $L(\phi)$ of basin 2 as a function of latitude and the southern extent of the peninsula dividing the two basins ϕ_S.

Because Eq. (18) is complex, it provides information about both the relative amplitude of the responses in each basin and the phase difference between them. Figure 3 shows the results for two identical sector ocean basins, each 50° wide and extending from 36°S to 65°N. Forcing periods of up to 250 yr are shown throughout this section to establish the implications of the theory right across parameter space. It is important to note, however, that on centennial time scales in the real ocean the thermodynamic part of the adjustment begins to play a role, and the low-frequency results shown here should be treated with caution.

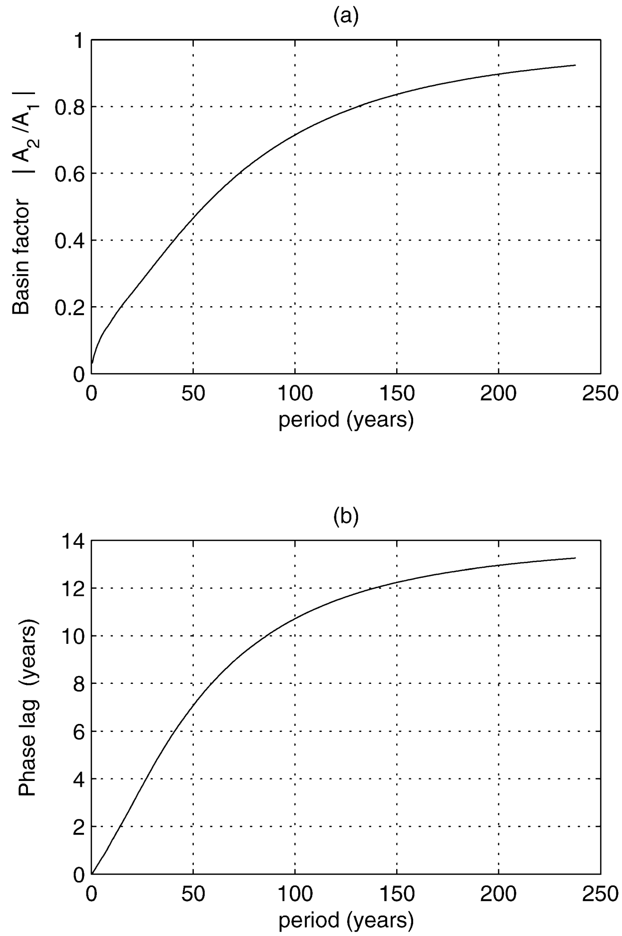

FIG. 3. (a) Magnitude and (b) phase of the ratio A_2/A_1, as a function of forcing period, for two identical sector ocean basins each 50° wide and extending from 36°S to 65°N.

In Fig. 3a the relative amplitude is plotted. At frequencies higher than 1/(50 yr) it varies approximately linearly with the period of the forcing—the longer the period, the larger the response in thermocline thickness on the eastern boundary of basin 2. Even for a forcing period of 50 yr, though, the response in this second basin is less than 50% of that in the forced basin 1. At low frequencies the ratio asymptotically approaches 1. This result implies that in the steady state the surface-layer thickness changes uniformly across both basins, a consequence of the fact that the only net flow into or out of the domain is the prescribed forcing T_{N1}, which must therefore be balanced by changes in layer thickness (i.e., changes in storage) within the domain itself.

Figure 3b shows the phase lag in years of the response in basin 2 behind that in basin 1. At high frequencies it too varies approximately linearly with the forcing period (about 15% of the period); in the low-frequency limit it asymptotically approaches a value of 13.3 yr.

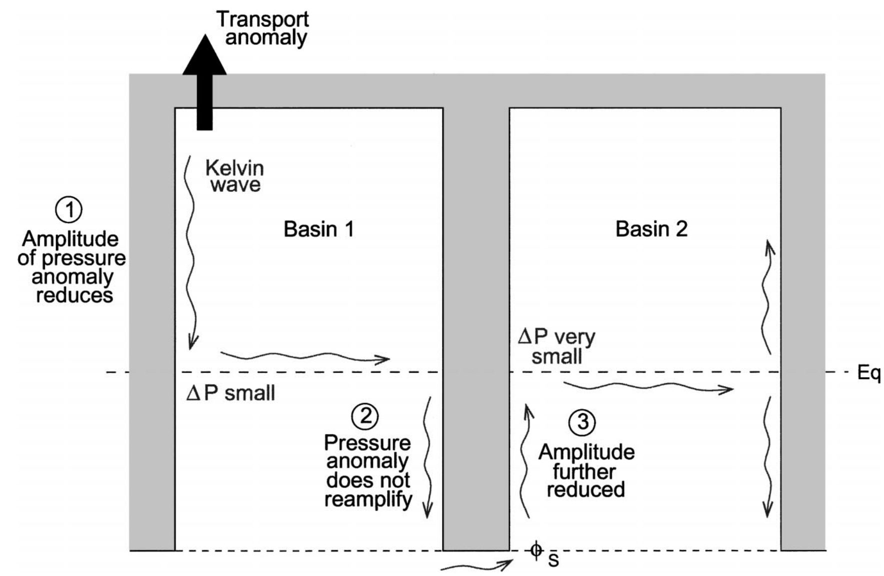

FIG. 4. Schematic illustrating the Kelvin wave response to a prescribed anomaly in thermohaline overturning on the northern boundary of basin 1. The associated pressure anomaly is in geostrophic balance and consequently reduces in amplitude as it propagates southward as a Kelvin wave along the western boundary (1). The resulting small thermocline displacement is transmitted across the equator but does not reamplify as the Kelvin wave travels poleward on the eastern side of basin 1 (2). Having propagated around the cape separating the two basins, the Kelvin wave is further reduced in amplitude as it travels equatorward along the western boundary of basin 2 (3). The response on the eastern boundary of basin 2 is therefore smaller than that on the eastern boundary of basin 1 and depends upon the latitude ϕ_S. Rossby waves communicate the reduced pressure anomaly into the interior of each basin.

This is the maximum Rossby wave transit time in the system (which in this idealized ocean geometry occurs on the northern boundary of each basin).

In physical terms, the eastern boundary response in basin 2 is smaller than the response in basin 1 because the anomaly in thermocline thickness, having propagated around the dividing land mass as a Kelvin wave, is reduced in amplitude as it travels equatorward in close to geostrophic balance along the western boundary of basin 2 (Johnson and Marshall 2002a and Fig. 4). One might imagine, therefore, that the closer the southern connection between ocean basins is to the equator, the larger the amplitude of variability will be in basin 2. This relationship is apparent in the variation of the basin factor $|A_2/A_1|$ with the southern extent of the dividing land mass (Fig. 5). If the zonal channel connecting two basins occurs exactly on the equator, there is no difference in the amplitude of variability between them.

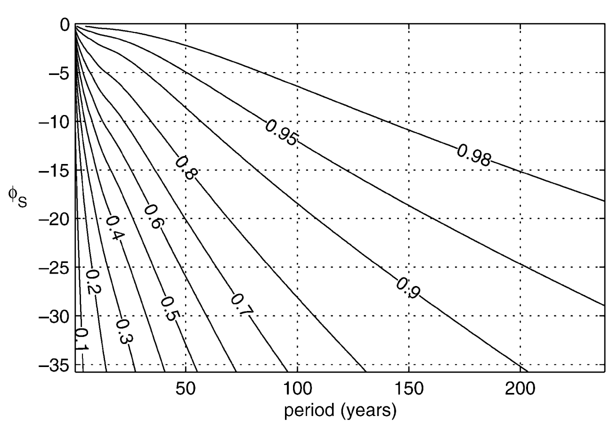

FIG. 5. Variation of the basin factor $|A_2/A_1|$ with frequency and with the southern extent of the dividing land mass ϕ_S.

b. Meridional overturning anomalies

Dividing Eq. (16) by T_{N1} and substituting for T_0 using Eq. (14) gives an expression for the amplitude of variability in meridional transport throughout basin 1:

$$\frac{T_1}{T_{N1}}(\phi, \omega) = \frac{\dfrac{g'H}{f_S}\left(1 - \dfrac{A_2}{A_1}\right) - \displaystyle\int_{\phi_S}^{\phi} Rc[1 - e^{(-i\omega L_1)/c}]\, d\phi}{\dfrac{g'H}{f_S}\left(1 - \dfrac{A_2}{A_1}\right) - \displaystyle\int_{\phi_S}^{\phi_N} Rc[1 - e^{(-i\omega L_1)/c}]\, d\phi}. \tag{19}$$

This equation is general—it does not rely upon the fact that the two basins are identical but applies to the case of any two basins that extend south of the equator to the same latitude ϕ_S.

Transport anomalies in basin 2 can be obtained by treating it as a single basin, forced on its southern boundary by the variability that remains after the amplitude of the signal has been reduced in basin 1. Dividing Eq. (17) by T_{S2}, and substituting using Eq. (15) gives

$$\frac{T_2}{T_{S2}}(\phi, \omega) = 1 - \frac{\displaystyle\int_{\phi_S}^{\phi} Rc[1 - e^{(-i\omega L_2)/c}]\, d\phi}{\displaystyle\int_{\phi_S}^{\phi_N} Rc[1 - e^{(-i\omega L_2)/c}]\, d\phi}, \quad (20)$$

where

$$T_{S2} = -T_1(\phi = \phi_S). \quad (21)$$

The minus sign here reflects the fact that any flow leaving basin 1 is assumed to enter basin 2. A southward anomaly in meridional transport on the southern boundary of basin 1 is equivalent to a northward anomaly in transport on the southern boundary of basin 2.

Figure 6 shows the numerical solution of Eqs. (19) and (20). Plotted is the amplitude of variability in meridional transport as a fraction of the prescribed variability on the northern boundary of basin 1. The single-basin solution from Fig. 1 is also plotted for comparison.

In the high-frequency limit, the basin factor $|A_2/A_1| \to 0$ (see Fig. 3), and Eq. (19) therefore reduces to the single-basin solution in Eq. (9). This fact is apparent in Fig. 6a and is as we might expect from section 2. High-frequency variability is confined to the North Atlantic as a result of the equatorial buffer mechanism, and so the presence of a second basin has little effect.

In contrast, low-frequency variability is able to pass across the equator with little reduction in amplitude. At low frequencies, reduction in the amplitude of transport anomalies with latitude is instead controlled by the dynamic boundary condition $T = 0$ at the northern margin of basin 2. The magnitude of the transport anomaly in both basins varies approximately linearly with latitude, with the amplitude in basin 2 decreasing northward and falling to zero at $\phi = \phi_N$ (the decrease is not exactly linear since basin width varies as the cosine of latitude). This is physically the result of storage in the surface layer.

The phase lag of the transport signal (in years) is shown in Fig. 7. In basin 1, divergence from the single-basin solution occurs at a relatively high frequency. For variability with a period longer than about 100 yr, the phase lag is independent of frequency and increases with distance from the forcing region on the northern boundary. In basin 2, the phase lag at high frequencies is only a weak function of latitude and increases approximately linearly with the period of the variability. In the low-frequency limit, it becomes a function simply of latitude, increasing northward throughout the domain.

Close to the northern boundary of basin 2, at a frequency corresponding to the transit time of a Rossby wave (~13 yr) and its harmonics, the phase lag drops to zero because of a resonance between the Rossby wave signal and the forcing on the western boundary, discussed for the single-basin case in section 2. The difference here is that western boundary "forcing" in basin 2 is not prescribed as a volume flux on the northern boundary but is determined by the mass balance of the whole basin. Resonance occurs at a frequency such that Rossby wave propagation at high latitudes generates Kelvin waves on the western boundary that will reinforce the eastern boundary thickness anomaly. The amplitude of variability on the northern boundary of basin 2 is so small, however, that the phase lag here means very little in real terms.

If the width of basin 2 vanishes ($L_2 \to 0$), then from Eq. (18) $A_2 = A_1$, and

$$\frac{T_1}{T_{N1}}(\phi, \omega) = \frac{\displaystyle\int_{\phi_S}^{\phi} Rc[1 - e^{(-i\omega L_1)/c}]\, d\phi}{\displaystyle\int_{\phi_S}^{\phi_N} Rc[1 - e^{(-i\omega L_1)/c}]\, d\phi}. \quad (22)$$

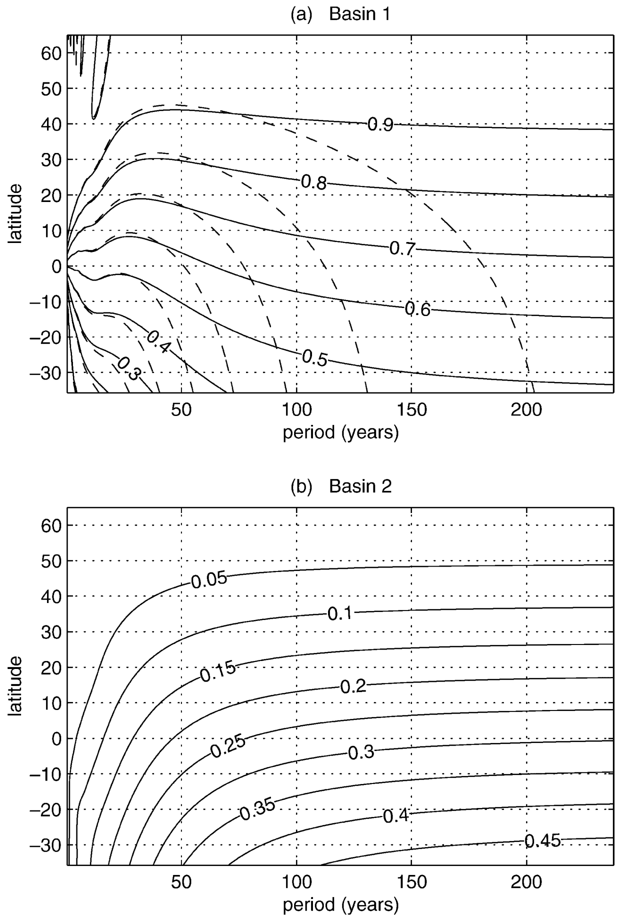

FIG. 6. Amplitude of the variability in meridional transport as a fraction of the prescribed variability on the northern boundary of basin 1, for each of two identical sector ocean basins ($|T/T_{N1}|$). The dashed contours show the equivalent for a single basin with an open southern boundary. At decadal frequencies, when variability is confined to the hemispheric basin in which it is generated, the two solutions in (a) basin 1 are identical, and (b) basin 2 experiences only a very small fraction of the variability.

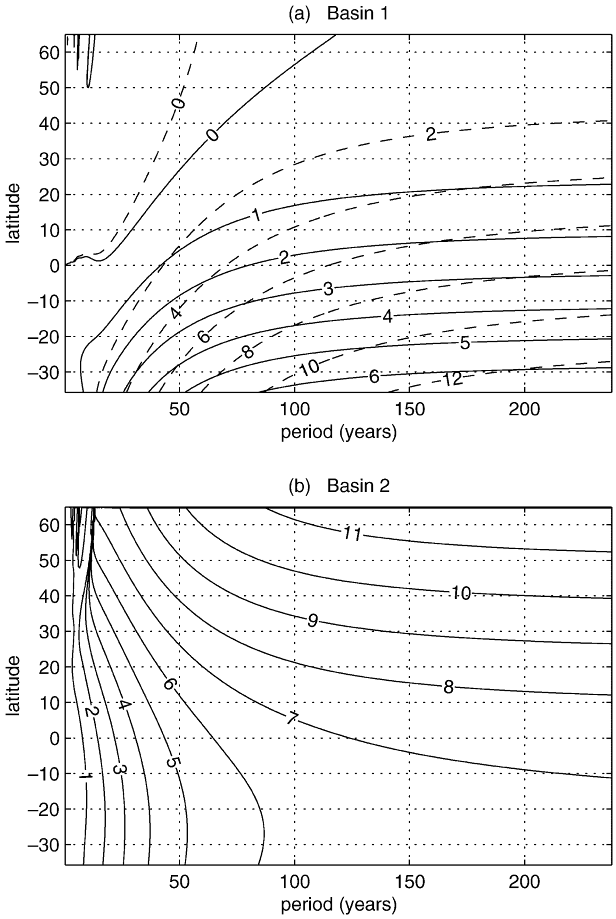

FIG. 7. Phase lag, in years, of the variability in transport at each latitude for each of two identical sector ocean basins, $\arg(T/T_{N1})$. The dashed contours in (a) show the single-basin case.

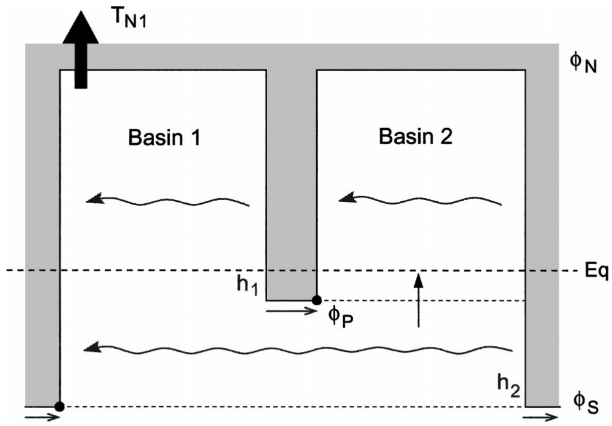

FIG. 8. The asymmetric two-basin case. Eastern boundary thickness anomalies in each basin are communicated to the next by Kelvin waves to the south of the dividing land mass. It is helpful to view basin 1 as an L-shaped basin, in which Rossby waves reaching the western side come from both the eastern boundary of basin 1 itself and, south of ϕ_P, from the eastern boundary of basin 2. The geostrophic flow shown by the straight arrow is a source to basin 2 and a sink to basin 1. There is no geostrophic flow into basin 1 from the south because the thickness on both sides of the basin is equal to h_2.

This expression differs from the equivalent result for the single-basin case in section 2 [Eq. (9)] because here there is no outflow on the southern boundary (T_S) and adjustment must occur entirely within the basin itself.

c. Asymmetric basins

When the land masses between the two ocean basins extend to different latitudes, the analysis becomes a little more complicated. Consider the case illustrated in Fig. 8, in which one land mass extends to ϕ_S as before, but the southern tip of the other occurs farther north at ϕ_P. It is helpful to view basin 1 as an L-shaped basin, in which the meridional transport depends upon Rossby wave propagation both from the east coast of basin 1 itself and, south of ϕ_P, from the east coast of basin 2. The mass budget equation integrated over the meridional extent of basin 1 will involve two integrated Rossby wave terms. If one assumes a periodic forcing and response, it becomes

$$T_0 + \frac{g'H}{f_P}(A_2 - A_1) + A_1 \int_{\phi_P}^{\phi_N} Rc[1 - e^{(-i\omega L_1)/c}]\, d\phi + A_2 \int_{\phi_S}^{\phi_P} Rc[1 - e^{(-i\omega L_1)/c}]\, d\phi = 0, \tag{23}$$

where A_1 and A_2 are the amplitudes of the variability in layer thickness on the eastern boundaries of basins 1 and 2, respectively. The second term here represents the flow out of the L-shaped basin 1 and into the closed basin 2. There is no geostrophic flow into basin 1 from the south because the layer thickness on both sides of the basin is h_2. Integrating over the meridional extent of basin 2 results in

$$-\frac{g'H}{f_P}(A_2 - A_1) + A_2 \int_{\phi_P}^{\phi_N} Rc[1 - e^{(-i\omega L_2)/c}]\, d\phi = 0. \tag{24}$$

This gives us the same basin factor as in section 3a, where now the Coriolis parameter is evaluated at the latitude ϕ_P:

$$\frac{A_2}{A_1} = \frac{\dfrac{g'H}{f_P}}{\dfrac{g'H}{f_P} - \displaystyle\int_{\phi_P}^{\phi_N} Rc[1 - e^{(-i\omega L_2)/c}]\, d\phi}. \tag{25}$$

Integrating the mass budget in basin 1 from its southern boundary up to a latitude ϕ, which lies in the closed portion of the basin, gives the transport T_1:

$$T_1 = -e^{i\omega t}\left\{\frac{g'H}{f_P}(A_2 - A_1) + A_1\int_{\phi_P}^{\phi} Rc[1 - e^{(-i\omega L_1)/c}]\,d\phi + A_2\int_{\phi_S}^{\phi_P} Rc[1 - e^{(-i\omega L_1)/c}]\,d\phi\right\}. \quad (26)$$

Using Eq. (23) this simplifies to

$$T_1 = A_1 e^{i\omega t}\int_{\phi}^{\phi_N} Rc[1 - e^{(-i\omega L_1)/c}]\,d\phi + T_0 e^{i\omega t}, \quad (27)$$

and in basin 2

$$T_2 = -e^{i\omega t}\left\{-\frac{g'H}{f_P}(A_2 - A_1) + A_2\int_{\phi_P}^{\phi} Rc[1 - e^{(-i\omega L_2)/c}]\,d\phi\right\} = A_2 e^{i\omega t}\int_{\phi}^{\phi_N} Rc[1 - e^{(-i\omega L_2)/c}]\,d\phi. \quad (28)$$

South of ϕ_P in basin 1, the transport anomaly at a latitude ϕ is

$$T_1 = -A_2 e^{i\omega t}\int_{\phi_S}^{\phi} Rc[1 - e^{(-i\omega L_1)/c}]\,d\phi, \quad (29)$$

determined only by Rossby wave propagation from the east coast. Transports T_1 and T_2 are again functions of latitude ϕ and frequency ω. Dividing Eqs. (27)–(29) by T_{N1} and substituting for T_0 using Eq. (23) gives the amplitude of variability in meridional transport as a fraction of the forcing. Figure 9 shows the result for the case where $\phi_P = 10°S$, $\phi_S = 36°S$, and $\phi_N = 65°N$. Both ocean basins are 50° wide, and the dividing land masses have negligible width. At decadal and multidecadal frequencies, the asymmetry between basins results in less of a reduction in the amplitude of overturning anomalies in basin 1 and a larger amplitude of variability north of the equator in basin 2 (as compared with the case of two identical basins). In the low-frequency limit, however, the storage dominates and the layer shallows uniformly throughout the domain such that north of ϕ_P the reduction in amplitude is approximately independent of the value of ϕ_P itself. A comparison of Figs. 9 and 6 illustrates this point. Note that there is a discontinuity in the northward transport in basin 1 at ϕ_P, where the basin doubles in width to encompass the area to the south of basin 2. The northward transport in basin 1 is discontinuous across ϕ_P to account for the northward transport from basin 1 into basin 2.

The only assumption required about the geometry of the domain in the analysis above is that ϕ_S is south of ϕ_P. The equation set is therefore equally applicable when ϕ_P falls north of the equator. In this case Kelvin waves propagate around the peninsula with the coast on their right-hand side, and the direction of information propagation is from basin 2 to basin 1. The analytical theory still holds because it assumes Kelvin wave propagation to be instantaneous. It relies only upon the fact that the layer thickness at the southwest corner of basin 2 is equal to that on the eastern boundary of basin 1 at all times. The theory is, in effect, an instantaneous mass balance of the surface layer, and, as a result, the direction of propagation of Kelvin waves is irrelevant.

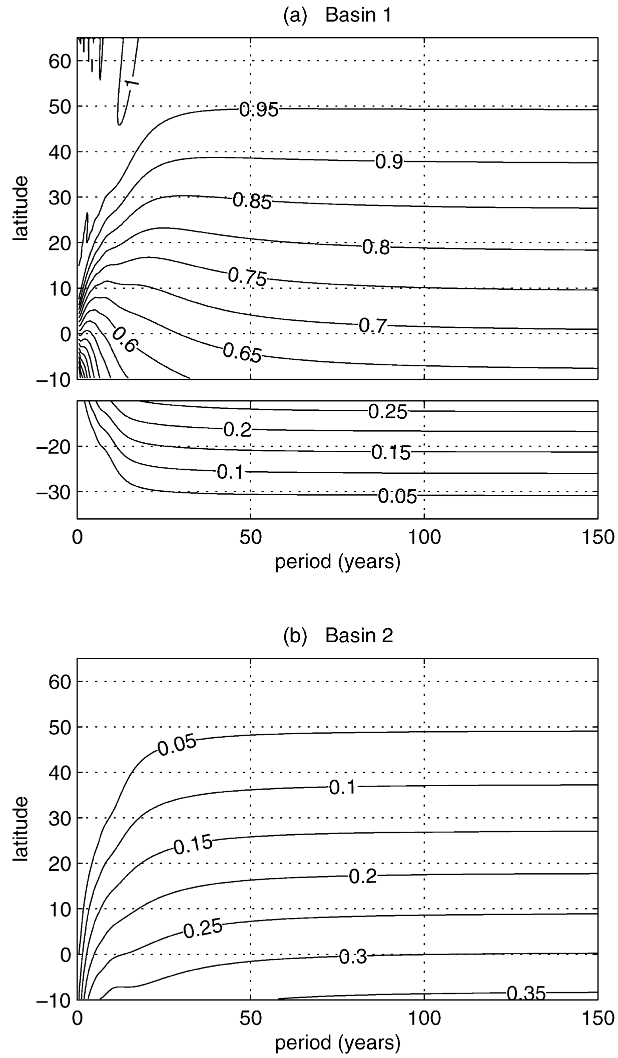

FIG. 9. Asymmetric basins—amplitude of the variability in meridional transport as a fraction of the prescribed variability on the northern boundary of basin 1.

Figure 10 shows the magnitude of the basin factor [Eq. (25)] as a function of ϕ_P and of frequency. When ϕ_P is south of the equator, $|A_2/A_1|$ is plotted (exactly as in Fig. 5), but, for ϕ_P north of the equator, the amplitude of variability in basin 2 is larger than that in basin 1 and the figure shows contours of $|A_1/A_2|$.

For peninsulas that do not extend far from the northern boundary of the model, and for peninsulas that extend almost to the equator, there is very little reduction

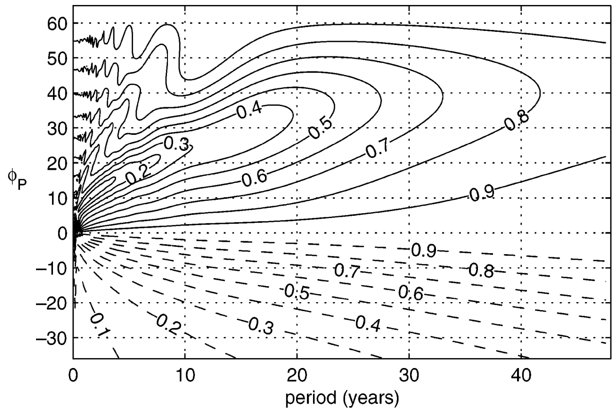

FIG. 10. Basin factor in the asymmetric case as a function of ϕ_P and frequency. For peninsulas south of the equator, the dashed contours show $|A_2/A_1|$. North of the equator, the solid contours show $|A_1/A_2|$, such that the basin factor is always <1.

in the eastern boundary signal between the two basins. For peninsulas of intermediate extent, however, the reduction in amplitude increases with frequency and is greater than 50% for variability with a period shorter than 25 yr. The latitude ϕ_P at which this maximum reduction in the eastern boundary signal occurs decreases with frequency.

In the real ocean, the only peninsula of significant meridional extent that is entirely contained within the Northern Hemisphere is the Indian peninsula, which separates the Arabian Sea and Bay of Bengal in the Indian Ocean. The 500-m isobath here extends to approximately 5°N. Only the dimensions of the Bay of Bengal are required to calculate the basin factor—the result is shown in Fig. 11. For variability with a period longer than about 3 yr the basin factor is very close to 1. Because at annual frequencies critical assumptions of the theory begin to break down in any case, for our purposes here eastern boundary thickness in the Bay of Bengal can be assumed to be equal to eastern boundary

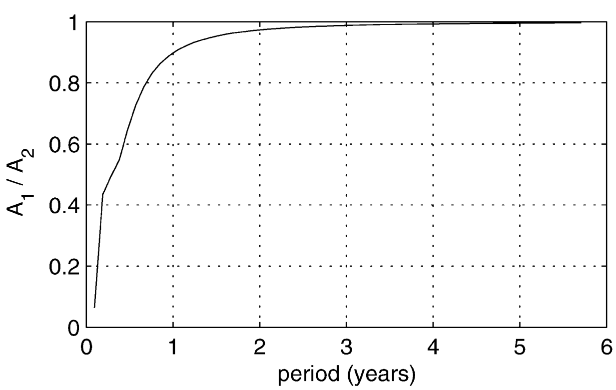

FIG. 11. Ratio of the amplitude of variability in layer thickness on the eastern boundary of the Arabian Sea (A_1) to that in the Bay of Bengal (A_2). At all frequencies for which the conceptual model is valid, the ratio is very close to 1.

thickness in the Arabian Sea, and the global ocean can be treated as three separate basins.

4. Global ocean geometry

Having demonstrated the multiple-basin approach using two idealized basins, we are now in a position to consider a more realistic global ocean geometry. This geometry is represented as three large ocean basins, connected via a circumpolar channel to the south, as illustrated in Fig. 12. Eastern boundary layer thickness and zonally integrated transport in each basin are labeled with the suffix A, I, or P for the Atlantic, Indian, and Pacific basins, respectively. The latitude of the southern tip of Africa is labeled ϕ_I, because it represents the southern extent of the closed portion of the Indian basin, and the latitude of the southern tip of Australasia, the most southerly extent of the Pacific basin, is similarly labeled ϕ_P. The tip of South America, Cape Horn, is ϕ_S, and the northern boundary of the Atlantic is ϕ_N. All three continents extend into the Southern Hemisphere, and so Kelvin waves propagate in the direction shown. The layer thickness in the southwest corner of each basin is equal, in our theoretical model, to the eastern boundary thickness in the basin immediately to the west. Ocean basins are defined by the 500-m isobath, the approximate edge of the continental shelf, and islands have been removed. It is assumed that Rossby waves impinging upon the eastern side of an island generate Kelvin waves around the coast and are then reradiated as Rossby waves from the western side (Liu et al. 1999). The ocean is forced on the northern boundary of the Atlantic, as before, with a periodic volume flux T_N whose mean is zero, intended to represent variability in deep-water formation at high latitudes.

The general equation

$$\frac{\partial}{\partial \phi}T(\phi, t) = Rc\left[h_e\left(t - \frac{L}{c}\right) - h_e(t)\right] \qquad (30)$$

is first integrated over the entire meridional extent of each basin. For this purpose the Atlantic ocean is assumed to be "staircase" shaped, such that the unbounded areas of ocean south of the Indian and Pacific basins are treated as part of the Atlantic (see Fig. 12). Zonally integrated flow into the Indian and Pacific basins is considered as a sink of Atlantic transport and is given by a linear geostrophic boundary condition as in section 3. There is no geostrophic flow across the latitude ϕ_S, because the layer thickness on both sides of Cape Horn is equal to h_P.

Integrals over the meridional extent of each basin result in the following balances:

$$-\frac{g'H}{f_P}(h_P - h_I) = \int_{\phi_P}^{\phi_N} Rc\left[h_P\left(t - \frac{L_P}{c}\right) - h_P(t)\right] d\phi, \qquad (31)$$

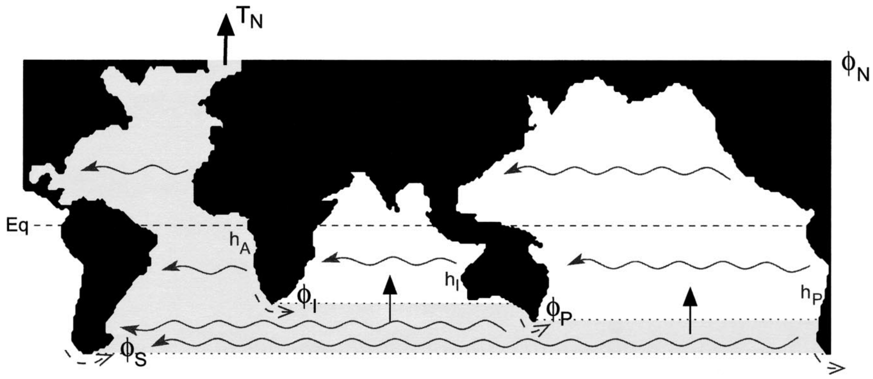

FIG. 12. Global ocean schematic. The direction of Kelvin wave propagation between basins is shown by dashed arrows. The Atlantic (shaded) is treated as staircase shaped and includes the unbounded areas of ocean to the south of the Indian and Pacific basins. Rossby waves (solid arrows) reaching its western side have propagated from three separate eastern boundary regions. The geostrophic flow into the Indian and Pacific basins is shown by bold face straight arrows. Basins are defined by the 500-m isobath; $\phi_N = 65°$N, $\phi_I = 36°$S, $\phi_P = 45°$S, and $\phi_S = 56°$S.

$$-\frac{g'H}{f_I}(h_I - h_A) = \int_{\phi_I}^{\phi_N} Rc\left[h_I\left(t - \frac{L_I}{c}\right) - h_I(t)\right] d\phi, \quad (32)$$

and

$$\begin{aligned} T_N &+ \frac{g'H}{f_P}(h_P - h_I) + \frac{g'H}{f_I}(h_I - h_A) \\ &= \int_{\phi_I}^{\phi_N} Rc\left[h_A\left(t - \frac{L_A}{c}\right) - h_A(t)\right] d\phi \\ &\quad + \int_{\phi_P}^{\phi_I} Rc\left[h_I\left(t - \frac{L_A}{c}\right) - h_I(t)\right] d\phi \\ &\quad + \int_{\phi_S}^{\phi_P} Rc\left[h_P\left(t - \frac{L_A}{c}\right) - h_P(t)\right] d\phi. \quad (33) \end{aligned}$$

Both the forcing and the response in each basin are assumed to be periodic, as before:

$$\begin{aligned} T_N &= T_0 e^{i\omega t}, \\ h_A &= h_0 + Ae^{i\omega t}, \\ h_I &= h_0 + Ie^{i\omega t}, \quad \text{and} \\ h_P &= h_0 + Pe^{i\omega t}, \quad (34) \end{aligned}$$

where A, I, and P are the amplitudes of variability in h_e in the Atlantic, Indian, and Pacific, respectively. After dividing through by $e^{i\omega t}$, Eqs. (31)–(33) become

$$\frac{g'H}{f_P}(P - I) = P\int_{\phi_P}^{\phi_N} Rc[1 - e^{(-i\omega L_P)/c}]\, d\phi, \quad (35)$$

$$\frac{g'H}{f_I}(I - A) = I\int_{\phi_I}^{\phi_N} Rc[1 - e^{(-i\omega L_I)/c}]\, d\phi, \quad \text{and} \quad (36)$$

$$\begin{aligned} T_0 &+ \frac{g'H}{f_P}(P - I) + \frac{g'H}{f_I}(I - A) \\ &= -A\int_{\phi_I}^{\phi_N} Rc[1 - e^{(-i\omega L_A)/c}]\, d\phi \\ &\quad - I\int_{\phi_P}^{\phi_I} Rc[1 - e^{(-i\omega L_A)/c}]\, d\phi \\ &\quad - P\int_{\phi_S}^{\phi_P} Rc[1 - e^{(-i\omega L_A)/e.}]\, d\phi. \quad (37) \end{aligned}$$

a. Basin factors

Equations (35) and (36) can be rearranged to give the ratio of the eastern boundary responses in adjacent basins:

$$\frac{P}{I} = \frac{\dfrac{g'H}{f_P}}{\dfrac{g'H}{f_P} - \displaystyle\int_{\phi_P}^{\phi_N} Rc[1 - e^{(-i\omega L_P)/c}]\, d\phi} \quad \text{and} \quad (38)$$

$$\frac{I}{A} = \frac{\dfrac{g'H}{f_I}}{\dfrac{g'H}{f_I} - \displaystyle\int_{\phi_I}^{\phi_N} Rc[1 - e^{(-i\omega L_I)/c}]\, d\phi}. \quad (39)$$

The ratio of the response in the Pacific to that in the Atlantic, P/A, can be found by multiplying these two expressions together. To calculate these ratios for the real global ocean, all that is required is the width of each basin as a function of latitude and the integral

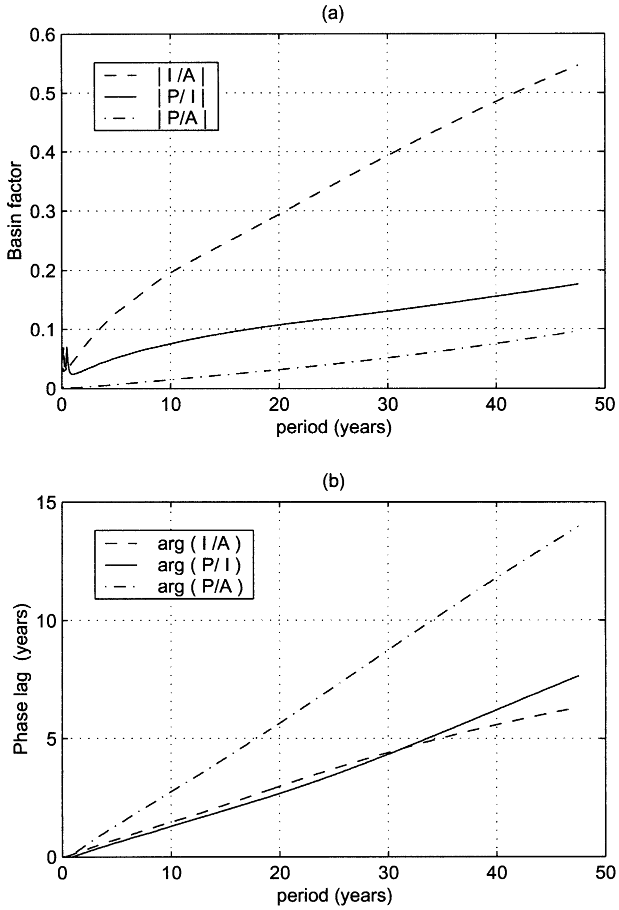

FIG. 13. (a) Relative amplitude of the variability in thermocline thickness on the eastern boundary of adjacent ocean basins. (b) Phase lag, in years.

limits $\phi_S = 56°S$, $\phi_P = 45°S$, $\phi_I = 36°S$, and $\phi_N = 65°N$.

Figure 13 shows the amplitude in each of the three cases (the basin factor introduced in section 3a) and the associated phase lag. In section 3 a wide range of frequencies was considered, but here attention is restricted to decadal and multidecadal frequencies.

All three basin factors increase as frequency decreases. For a forcing in the North Atlantic with a period of 40 yr, 50% of the variability in thermocline thickness is transmitted to the Indian Ocean, and only 8% to the Pacific. This justifies the assumption, made in section 2 and in Johnson and Marshall (2002a,b) for the single Atlantic basin case, that layer thickness h_{SW} in the southwest corner of the domain is constant, because signals propagating back into the Atlantic from the Pacific at decadal frequencies are small. The basin factors all asymptotically approach 1, consistent with a steady-state solution of uniform shallowing throughout the domain. After 155 yr $|I/A| > 0.9$, and $|P/A| > 0.9$ after 642 yr. These time scales suggest that adjustment times for the global ocean basins are additive rather than multiplicative; that is, despite being subject to equatorial "buffers" in three ocean basins, the adjustment of the Pacific by Rossby waves from the eastern boundary occurs over centuries rather than millenia. The phase lag of the variability in the Pacific behind that in the Atlantic is approximately 30% of the forcing period over the range of frequencies shown here.

Huang et al. (2000) consider the steady-state change in the global thermocline after adjustment to a sudden change in the prescribed high-latitude Atlantic forcing. They find that the thermocline in the Indian basin adjusts by 83% of the change in the Atlantic and that the Pacific thermocline undergoes an adjustment of 44%. Their experiment is not directly comparable with the results reported here because of 1) their emphasis on the steady-state solution (the time-dependent adjustment is not considered), 2) the distributed source that they apply as a forcing, and 3) their inclusion of a simple Rayleigh reduction term to represent the diabatic adjustment, which is not included in our model. However, their steady-state results are qualitatively similar to the change in thermocline thickness found here, at the multidecadal frequencies comparable to their damping time scale. Huang et al. (2000) also find that, when friction is increased, thermocline perturbations become increasingly confined to the Atlantic Ocean. This result is consistent with the model suggested here, because adjustment in other basins relies upon Kelvin wave propagation, which is subject to dissipation.

b. Meridional overturning anomalies

Integrating Eq. (30) from the southern extent of each basin up to a latitude ϕ leads to a set of expressions for the zonally integrated transport at any point in the global ocean:

$$T_P(\phi) = e^{i\omega t}\left\{\frac{g'H}{f_P}(P - I) - P\int_{\phi_P}^{\phi} Rc[1 - e^{(-i\omega L_P)/c}]\,d\phi\right\}, \tag{40}$$

$$T_I(\phi) = e^{i\omega t}\left\{\frac{g'H}{f_I}(I - A) - I\int_{\phi_I}^{\phi} Rc[1 - e^{(-i\omega L_I)/c}]\,d\phi\right\}, \tag{41}$$

$$T_A(\phi_I < \phi < \phi_N) = -e^{i\omega t}\left\{\frac{g'H}{f_P}(P - I) + \frac{g'H}{f_I}(I - A) + A\int_{\phi_I}^{\phi} Rc[1 - e^{(-i\omega L_A)/c}]\, d\phi + I\int_{\phi_P}^{\phi_I} Rc[1 - e^{(-i\omega L_A)/c}]\, d\phi + P\int_{\phi_S}^{\phi_P} Rc[1 - e^{(-i\omega L_A)/c}]\, d\phi\right\}, \quad (42)$$

$$T_A(\phi_P < \phi < \phi_I) = -e^{i\omega t}\left\{\frac{g'H}{f_P}(P - I) + I\int_{\phi_P}^{\phi} Rc[1 - e^{(-i\omega L_A)/c}]\, d\phi + P\int_{\phi_S}^{\phi_P} Rc[1 - e^{(-i\omega L_A)/c}]\, d\phi\right\}, \quad \text{and} \quad (43)$$

$$T_A(\phi_S < \phi < \phi_P) = -Pe^{i\omega t}\int_{\phi_S}^{\phi} Rc[1 - e^{(-i\omega L_A)/c}]\, d\phi. \quad (44)$$

The first three of these balances can be simplified considerably using Eqs. (35)–(37) to become

$$T_P(\phi) = Pe^{i\omega t}\int_{\phi}^{\phi_N} Rc[1 - e^{(-i\omega L_P)/c}]\, d\phi, \quad (45)$$

$$T_I(\phi) = Ie^{i\omega t}\int_{\phi}^{\phi_N} Rc[1 - e^{(-i\omega L_I)/c}]\, d\phi, \quad \text{and} \quad (46)$$

$$T_A(\phi_I < \phi < \phi_N) = Ae^{i\omega t}\int_{\phi}^{\phi_N} Rc[1 - e^{(-i\omega L_A)/c}]\, d\phi + T_0 e^{i\omega t}. \quad (47)$$

The process of dividing Eqs. (43)–(47) by $T_N = T_0 e^{i\omega t}$, substituting for T_0 using Eq. (37), and making use of the basin factors in Eqs. (38) and (39) allows the ratios T_A/T_N, T_I/T_N, and T_P/T_N to be determined.

The theoretical analysis above relies only upon the fact that

$$\phi_S < \phi_P < \phi_I < \phi_N. \quad (48)$$

It would apply even if one or more of the connections between ocean basins was in the Northern Hemisphere rather than in the Southern Hemisphere. To calculate the amplitude of thermohaline overturning anomalies in a realistic global ocean geometry requires only the width of each basin as a function of latitude and the values of ϕ_N, ϕ_I, ϕ_P, and ϕ_S. Figure 14 shows the modulus $|T/T_N|$ for each basin.

In the Atlantic itself the reduction in amplitude of overturning anomalies is almost identical to the single-basin case. This suggests, again, that fixing the surface-layer thickness h_{SW} in the southwest corner of the domain is a reasonable approximation if we are only interested in variability within the Atlantic sector. Region 4, between 36° and 45°S, demonstrates the fast adjustment that occurs in parts of the basin that do not cross the equator. It is bounded by geostrophic flows to the north and south and exhibits almost no variation in the amplitude of the transport signal with latitude. In the North Pacific and Indian basins, high-frequency signals are greatly reduced in amplitude—the low-pass filtering of the equator at work. At low frequencies the amplitude of anomalies in these basins varies approximately linearly with latitude, falling to zero on the closed northern boundary, because the storage term dominates. In the Pacific case, the amplitude of variability becomes linear at a much lower frequency—this basin is both wider and extends farther to the north, increasing the time taken for Rossby waves to cross the basin.

Only a tiny proportion of variability in the high-latitude North Atlantic is transmitted to the Southern Ocean (see region 5), which suggests that, on decadal and multidecadal time scales, variability in North Atlantic deep-water formation and in Southern Ocean processes is unlikely to be connected, unless it is through large-scale atmospheric forcing. However, the Southern Ocean does include sensitive convective regions, and it is possible that even a small signal could change the stratification around Antarctica by enough to affect deep-water formation and, hence, the local overturning circulation.

A weak resonance is apparent in the Southern Ocean as well as in the North Atlantic. The Rossby wave propagation time along what is almost an entire latitude circle in the Southern Ocean is approximately 70 yr. If our simple global model were to be forced on its southern boundary, where in the real ocean there is considerable variability, this resonance could play an important role.

Figure 15 shows the length of time in years by which the signal lags the forcing. In the South Atlantic it appears to vary almost linearly with both forcing period and latitude for the frequency range shown here. It agrees well with the single-basin case discussed in section 2. The phase lag in the Indian basin exhibits a maximum of about 2 yr (at all latitudes) for variability with a period of 35 yr. In the Pacific, phase lags are much longer. They continue to increase as the frequency decreases, and they are largest at about 40°N, the latitude at which Rossby wave propagation time reaches a maximum. (North of 40°N, although the Rossby wave speed continues to decrease, the narrowing in basin width dominates, and the transit time falls.) The phase lag in

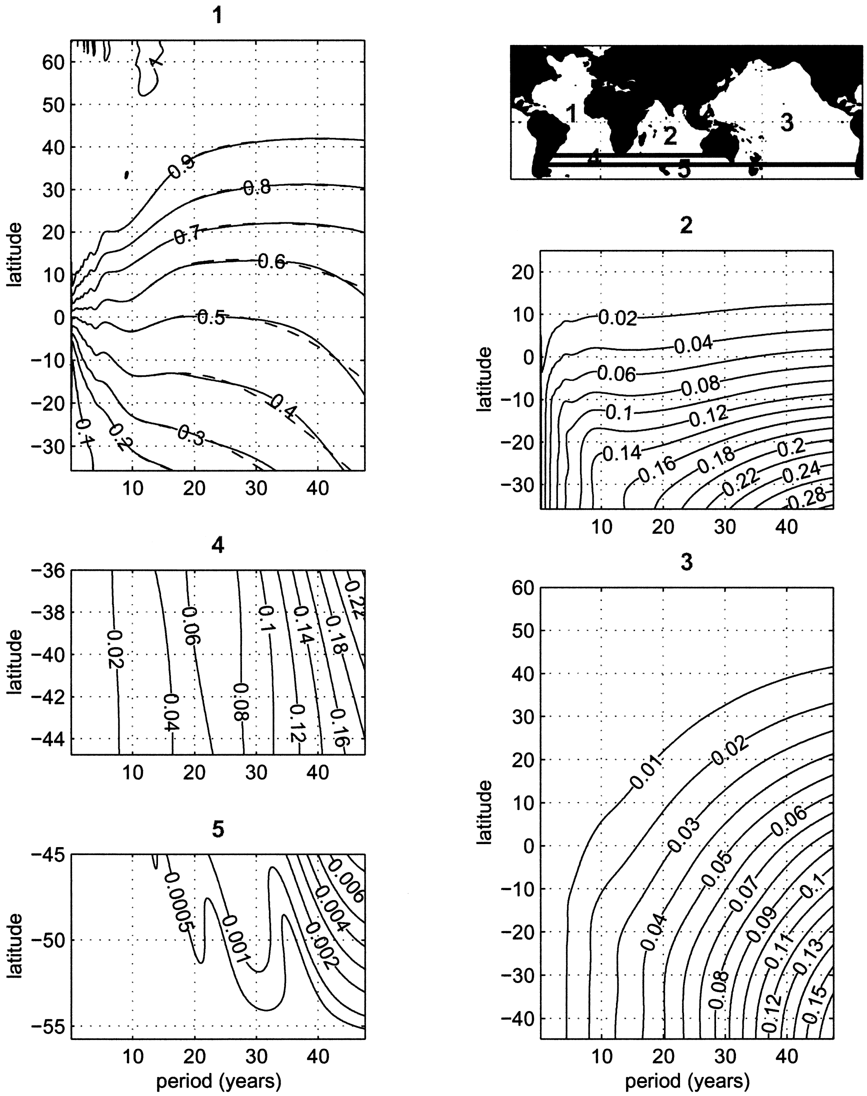

FIG. 14. Amplitude of the variability in zonally integrated meridional transport in each basin as a fraction of the prescribed transport variability on the northern boundary of the Atlantic. Each panel corresponds to a numbered region in the schematic (top right). The dashed lines in the Atlantic panel illustrate the single-basin case, in which layer thickness (h_{SW}) in the southwest corner of the domain is fixed.

the interval $\phi_S < \phi < \phi_P$ is not shown because here the amplitude of overturning anomalies is so small that the phase is practically meaningless.

We might expect the phase lag between basins in the real ocean to be somewhat longer than shown here, as a result of the time scale separation that is implicit in the theory. Kelvin waves propagating along boundaries and the equator are assumed to travel at infinite speeds, whereas in reality it will take a Kelvin wave about a year to reach the eastern boundary of the Indian Ocean from the North Atlantic forcing region and a further year to reach the eastern boundary of the Pacific.

Throughout the above, the Indian Ocean has been treated as a single basin. As discussed in section 3, its northern part in fact consists of two subbasins, the Arabian Sea and the Bay of Bengal, separated by the Indian peninsula, which extends to about 5°N. A similar analysis to that carried out in this section can be conducted that distinguishes the Arabian Sea and the Bay of Bengal, treating the global ocean as four basins instead of three. The resulting equations are considerably more complex and are not shown here, but the basin factors and the variability in zonally integrated transport in each basin are virtually indistinguishable (not shown). This result is as we might expect, because, at all but the highest frequencies, the basin factor for the Bay of Bengal is equal to 1 (Fig. 11). It justifies our treatment of the Indian Ocean as a single basin, with its width in the

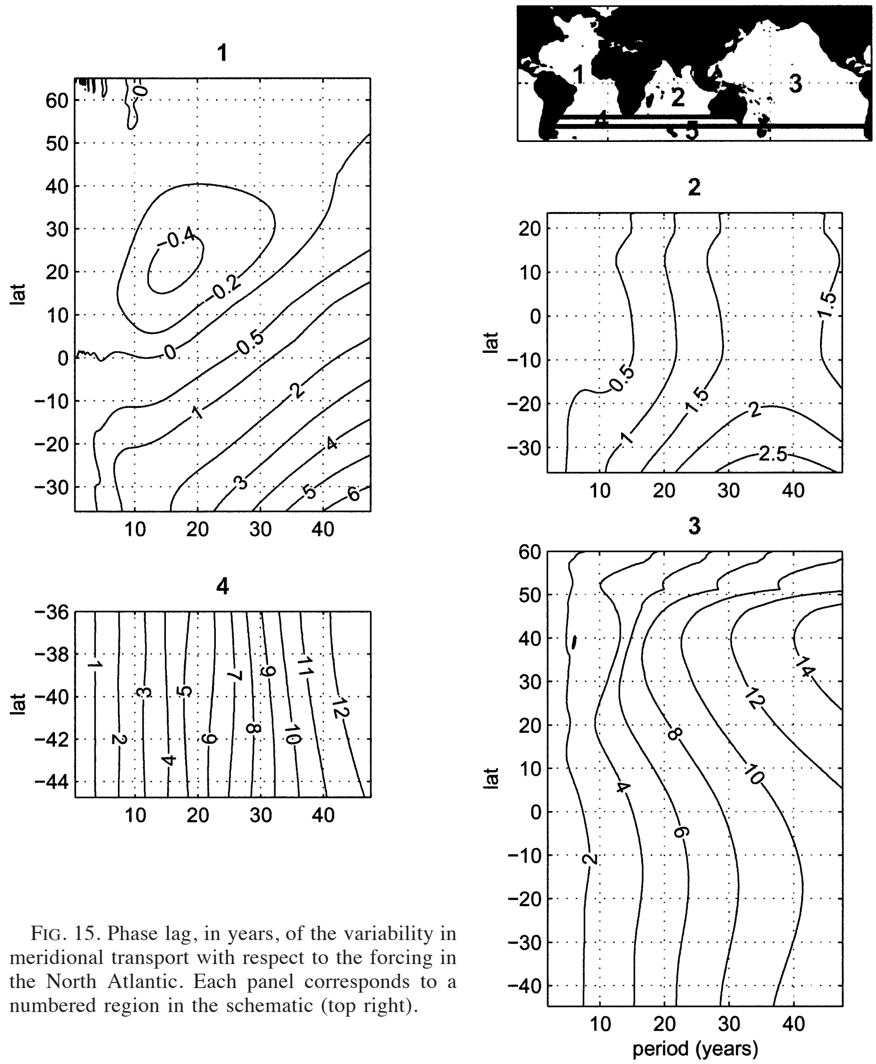

FIG. 15. Phase lag, in years, of the variability in meridional transport with respect to the forcing in the North Atlantic. Each panel corresponds to a numbered region in the schematic (top right).

northern portion equal to the width of the Arabian Sea plus the width of the Bay of Bengal.

The theory demonstrates, then, that at decadal frequencies variability in deep-water formation in the high-latitude North Atlantic has only a small effect on meridional transport in the Indian and Pacific Oceans. This is a consequence of the equatorial buffers that exist in each basin.

c. Numerical validation

To ensure that the theory developed here for thermohaline overturning anomalies in multiple basins has not diverged significantly from the physical model on which it is based, the shallow-water model described in Johnson and Marshall (2002a) is run in a realistic global ocean domain, at a resolution of 1°. This is an important check on the mechanisms involved, because, unlike the theory, the fully nonlinear numerical model explicitly represents the fast Kelvin wave response in each basin. Although Kelvin waves are not properly resolved at a resolution of 1°, on a C grid their propagation speed is unaffected (Hsieh et al. 1983). The model, initially at rest, is forced by a sinusoidal volume flux on the northern boundary of the Atlantic. The forcing has a period of 20 yr and an amplitude of 2 Sv (1 Sv $\equiv 10^6$ m^3 s^{-1}). The northern boundaries of the Indian and Pacific basins are closed. A periodic boundary condition is applied in the Southern Ocean so that the model includes a circumpolar channel extending from 56° to 65°S, with a solid boundary to its south. Elsewhere, the ocean geometry is defined by the 500-m isobath and is identical to that in Fig. 12. No-slip boundary conditions are imposed, and unresolved subgrid-scale processes are parameterized by harmonic diffusion terms in the momentum equations.

Figure 16 shows the average surface-layer thickness on the eastern boundary of the Atlantic, Indian, and Pacific basins over a 150-yr model run. The amplitude of the variability is in the ratio 1:0.28:0.03. This ratio

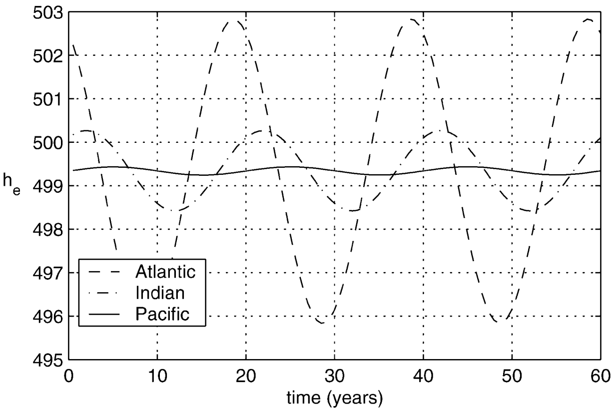

FIG. 16. Average surface-layer thickness on the eastern boundary of the Atlantic, Indian, and Pacific basins, diagnosed from a 1° global shallow-water model that is forced sinusoidally on the northern boundary of the Atlantic with a period of 20 yr and an amplitude of 2 Sv.

agrees well with the basin factors shown in Fig. 13a for a forcing period of 20 yr. In Fig. 16 the signal in the Indian basin lags that in the Atlantic by 3.2 yr, and that in the Pacific lags by a further 3 yr. These phase lags are slightly longer than those predicted by the theory (and shown in Fig. 13b), as we might expect from a numerical model that explicitly represents Kelvin waves.

In Fig. 17, the zonally integrated meridional transport in each basin is plotted as a function of latitude and time for 60 yr of the model run. The amplitude of the variability agrees very well with the theory in all three ocean basins. Approximately 25% of the variability in forcing is transmitted to the South Atlantic at 30°S, with only 5% and 2.5% reaching the equator in the Indian and Pacific Oceans, respectively. The phase lag throughout is again somewhat larger than theory predicts (by ~1 yr). At all latitudes in the Indian Ocean the signal lags the forcing by about 3 yr; in the Pacific the lag is almost 7 yr on the southern boundary, increasing to a maximum of 10 yr in the northern midlatitudes. (Note that a northward transport anomaly in the Atlantic Ocean becomes a southward anomaly in the Indian and Pacific Oceans).

For overturning anomalies with a period of 20 yr, then, the numerical modeling results appear to be described well by the theory. Figure 18 demonstrates that this is also true over a broader range of frequencies. It shows the basin factors diagnosed from further shallow-water model experiments in which the forcing has a period of 10, 30, and 40 yr. The theoretical curves are also plotted, and agreement is good.

d. Indonesian Throughflow

In the above analysis, it has been assumed that the fast Kelvin wave connection between the Indian and Pacific basins occurs around the southern edge of Australia. This interpretation is most likely appropriate for the deep limb of the MOC, but for the surface limb it is necessary to consider the possibility that Kelvin waves traveling along the eastern boundary of the Indian Ocean are transmitted to the Pacific via the Indonesian Throughflow region, much closer to the equator at 9°S.

With the Indonesian Throughflow open, Australia must be treated as a large island. Rossby waves impinging on it are assumed to generate coastal Kelvin waves and then to reradiate Rossby waves again from its western side. In contrast to section 4b,

$$\phi_S < \phi_I < \phi_P < \phi_N, \tag{49}$$

and so it now is helpful to view the Pacific Ocean as a closed basin, with both the Indian and Atlantic Oceans as "L-shaped" basins extending to the east. The resulting analytical expressions are more complicated, although the philosophy is the same.

A larger proportion of the variability reaches the Pacific at all frequencies with the Indonesian Throughflow open (not shown). This is due to the fact that Kelvin waves from the Indian Ocean arrive in the Pacific much closer to the equator. They therefore travel a shorter distance equatorward along the western boundary, and their amplitude is not as reduced (see Fig. 4). The effect of opening the Indonesian Throughflow on other ocean basins is small. Southern Ocean meridional transport varies by slightly more, and variability in the Indian basin now reaches a maximum for a forcing period of 8 yr. The Atlantic is barely affected at all. These results support those of Huang et al. (2000) who find that when the Indonesian Throughflow is open the steady-state thermocline displacement is larger in the Pacific and reduced in the Indian Ocean. However, because the deep modal expansion assumed throughout this study is not suitable for capturing the dynamics of shallow seas and flow across sills, the conclusions drawn here should be viewed as preliminary.

5. Concluding remarks

In this paper we have developed a linear theory for the propagation of meridional transport anomalies in a reduced-gravity ocean, consisting of multiple connected basins. Our key findings are the following.

- The equator acts as a low-pass filter to MOC anomalies.
- As a consequence, on decadal and shorter time scales, anomalies in MOC are confined to the hemispheric basin in which they are generated. Although fast Kelvin wave propagation along boundaries and the equator allows for the possibility of rapid communication between ocean basins, the amplitude of the response in surface-layer thickness and in the overturning circulation itself is small beyond the original basin.
- Damped basin modes are resonated by prescribed MOC anomalies, but only very weakly.

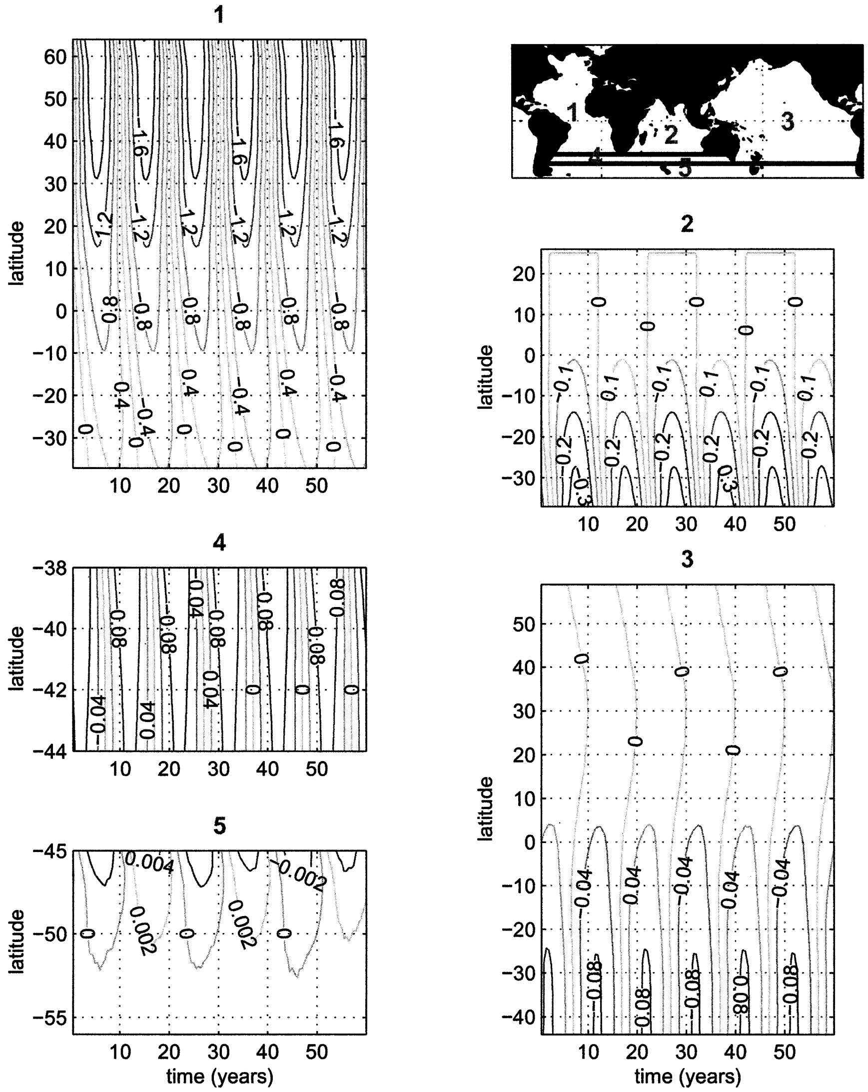

FIG. 17. Zonally integrated meridional transport in each basin as a function of latitude and time, diagnosed from a 1° global shallow-water model that is forced sinusoidally on the northern boundary of the Atlantic with a period of 20 yr and an amplitude of 2 Sv. Each panel corresponds to a numbered region in the schematic (top right).

- The results of full numerical integrations of the reduced-gravity equations can be reproduced, to excellent approximation, by a linear analytical theory that involves just one variable for each ocean basin.

We have found that MOC anomalies on interannual to decadal time scales are confined to the basin in which they are generated, but it is important to emphasize that they may still have a global impact through atmospheric teleconnections. For example, in a recent climate model experiment in which the North Atlantic MOC is shut down abruptly by an impulsive salinity forcing applied at high latitudes (Dong and Sutton 2002), the equatorial ocean circulation responds within a few months through the passage of a Kelvin wave. Over the next two years, an SST dipole anomaly is established across the tropical Atlantic, with cooling in the North Atlantic. This SST dipole anomaly, in turn, leads to a southward shift of the ITCZ, inducing a global atmospheric response within a few years. These global changes in atmospheric circulation may themselves induce further MOC anomalies in remote basins.

We regard the calculation presented here as a preliminary step toward a more detailed understanding of the teleconnections of MOC anomalies. There are many processes that have been neglected in this study but may play an important role in the ocean. For example, background mean flows will Doppler shift the higher baroclinic modes (e.g., Liu 1999; Killworth and Blundell

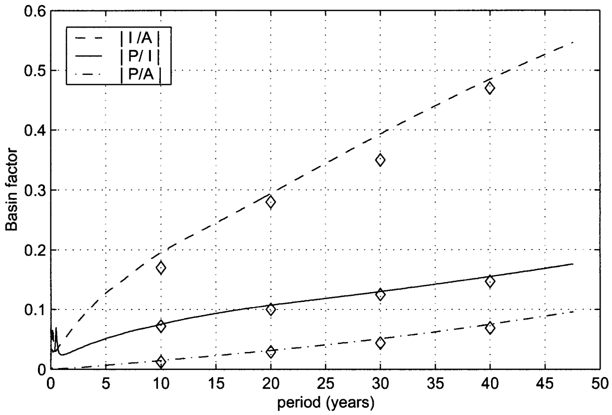

FIG. 18. Basin factors diagnosed from four global shallow-water model experiments, with forcing periods of 10, 20, 30, and 40 yr. The plotted curves show the theoretical predictions.

2001), thus modifying the details of the adjustment for these higher modes. Variable bottom topography may modify the propagation of MOC anomalies in several respects, including allowing the boundary adjustment to occur through coastal-trapped waves rather than Kelvin waves (Huthnance 1978), interactions between different baroclinic modes (if indeed such a modal decomposition makes sense; see Hallberg 1997), excitation of large-amplitude barotropic recirculations through interactions between the stratification and the bottom topography (the so-called JEBAR effect; e.g., Greatbatch et al. 1991; Häkkinen 2001; Gerdes and Köberle 1995), and possibly a blurring of the distinction between western and eastern boundaries. [However, we note that the calculations of Karcher (1997), employing an inverted shallow-water model over a realistic North Atlantic bottom topography, are essentially consistent with the adjustment mechanisms at the heart of the present theory.] Various eastern boundary processes such as coastal upwelling, surface mixing along the eastern boundary, and the Mediterranean outflow may also influence the poleward propagation of Kelvin waves and, hence, the propagation of MOC anomalies. Some models suggest that advection may be important in the adjustment process (e.g., Gerdes and Köberle 1995), and we note that advective effects will not be properly represented in the model used here because of the single active layer and the lack of a background mean flow. These issues will all require further study. Nevertheless we believe that many qualitative features of the theory we have developed for the propagation of MOC anomalies are likely to carry over to the ocean, even if the details of the theory may need modification.

Acknowledgments. This work was funded by the U.K. National Environment Research Council (NER/B/S/2001/00323). We are grateful to two anonymous reviewers for their insightful comments and suggestions.

APPENDIX

Analytical Solution on a β Plane

Under certain assumptions, Eq. (9) can be solved analytically. Aside from intellectual curiosity, this solution is useful in establishing the validity of the presented results and in ensuring that there are no unforeseen numerical effects.

As a complex fraction, Eq. (9) can be expressed in the form

$$\frac{T(\phi, \omega)}{T_N} = \frac{p + iq}{r + is}, \tag{A1}$$

where

$$p(\phi, \omega) = \frac{g'H}{f_S} - \int_{\phi_S}^{\phi} Rc\left[1 - \cos\left(\frac{\omega L}{c}\right)\right] d\phi, \tag{A2}$$

$$q(\phi, \omega) = -\int_{\phi_S}^{\phi} Rc \sin\left(\frac{\omega L}{c}\right) d\phi, \tag{A3}$$

$$r(\omega) = \frac{g'H}{f_S} - \int_{\phi_S}^{\phi_N} Rc\left[1 - \cos\left(\frac{\omega L}{c}\right)\right] d\phi, \tag{A4}$$

and

$$s(\omega) = -\int_{\phi_S}^{\phi_N} Rc \sin\left(\frac{\omega L}{c}\right) d\phi. \tag{A5}$$

Obtaining an analytical solution thus reduces to evaluating the two integrals:

$$\int_{\phi_S}^{\phi} c \cos\left(\frac{\omega L}{c}\right) d\phi \quad \text{and} \tag{A6}$$

$$\int_{\phi_S}^{\phi} c \sin\left(\frac{\omega L}{c}\right) d\phi. \tag{A7}$$

We now assume that the basin width L is constant, and we adopt a β plane such that the Rossby wave speed is inversely proportional to the square of the latitude:

$$c = \frac{\kappa}{\phi^2}, \tag{A8}$$

where $\kappa = g'H/\beta R^2$ and β is the meridional gradient in the Coriolis parameter (now taken to be constant with latitude). Equations (A6) and (A7) can then be integrated by parts to give

$$\int_{\phi_S}^{\phi} \frac{\kappa}{\phi^2} \cos\left(\frac{\omega L}{\kappa}\phi^2\right) d\phi = \left[-\frac{\kappa}{\phi}\cos\left(\frac{\omega L}{\kappa}\phi^2\right)\right]_{\phi_S}^{\phi} - \int_{\phi_S}^{\phi} 2\omega L \sin\left(\frac{\omega L}{\kappa}\phi^2\right) d\phi \quad \text{and}$$

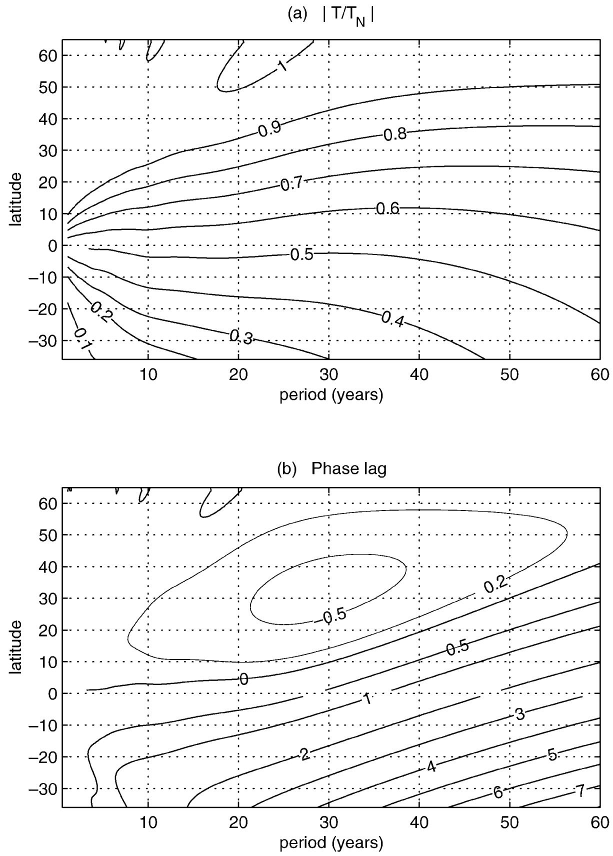

FIG. A1. Analytical solution of Eq. (9) for a constant basin width L and a Rossby wave speed given by κ/ϕ^2. (a) Modulus $|T/T_N|$, which gives the amplitude of the variability in meridional transport as a fraction of the prescribed variability on the northern boundary. (b) Phase lag $\arg(T/T_N)$, in years. This figure is not directly comparable with Fig. 1 but is encouragingly similar.

$$\int_{\phi_S}^{\phi} \frac{\kappa}{\phi^2} \sin\left(\frac{\omega L}{\kappa}\phi^2\right) d\phi$$
$$= \left[-\frac{\kappa}{\phi} \sin\left(\frac{\omega L}{\kappa}\phi^2\right)\right]_{\phi_S}^{\phi} + \int_{\phi_S}^{\phi} 2\omega L \cos\left(\frac{\omega L}{\kappa}\phi^2\right) d\phi.$$

The second term on the right-hand side in each case takes the form of a Fresnel integral. Fresnel integrals are defined as

$$C(x) = \int_0^x \cos\left(\frac{\pi}{2}t^2\right) dt \quad \text{and}$$
$$S(x) = \int_0^x \sin\left(\frac{\pi}{2}t^2\right) dt. \qquad \text{(A9)}$$

Under the appropriate transformation

$$t = \sqrt{\frac{2\omega L}{\pi\kappa}}\phi, \qquad \text{(A10)}$$

p and q become

$$p = \frac{g'H}{f_S} + R\left[\frac{\kappa}{\phi}\left\{1 - \cos\left(\frac{\omega L}{\kappa}\phi^2\right)\right\}\right]_{\phi_S}^{\phi}$$
$$- \sqrt{2\omega L\pi\kappa}R\left[\int_0^{x_S} \sin\left(\frac{\pi}{2}t^2\right) dt \pm \int_0^{x} \sin\left(\frac{\pi}{2}t^2\right) dt\right] \qquad \text{(A11)}$$

and

$$q = R\left[\frac{\kappa}{\phi} \sin\left(\frac{\omega L}{\kappa}\phi^2\right)\right]_{\phi_S}^{\phi}$$
$$- \sqrt{2\omega L\pi\kappa}R\left[\int_0^{x_S} \cos\left(\frac{\pi}{2}t^2\right) dt \pm \int_0^{x} \cos\left(\frac{\pi}{2}t^2\right) dt\right], \qquad \text{(A12)}$$

where $x = t = \sqrt{(2\omega L)/(\pi\kappa)}\phi$ at the latitude of interest ϕ, and x_S is the value of t on the southern boundary of the domain. Note that, because Fresnel integrals are defined from 0 to positive x, in our case the integrals must be split into two parts, each defined from the equator poleward. The "plus" applies if the latitude of interest is in the Northern Hemisphere, and the "minus" applies if it is in the Southern Hemisphere. Similar expressions follow for r and s.

Figure A1 shows the amplitude of variability $|T/T_N|$ and the phase lag $\arg(T/T_N)$ calculated using the analytical solution, with the parameters $L = 5.5 \times 10^6$ m and $\kappa = 0.01$ m s^{-1}. Although this figure is not directly comparable with the numerical solution in Fig. 1 because of the assumptions of a constant basin width and a Rossby wave speed given by κ/ϕ^2, the two figures are encouragingly similar. The resonance effects toward the north of the domain, noted already in the numerical solution, are perhaps not surprising given the oscillatory nature of the Fresnel integrals.

REFERENCES

Broecker, W., and G. H. Denton, 1989: The role of ocean–atmosphere reorganizations in glacial cycles. *Geochimica et Cosmochimica Acta,* **53,** 2465–2501.

Cessi, P., and S. Louazel, 2001: Decadal oceanic response to stochastic wind forcing. *J. Phys. Oceanogr.,* **31,** 3020–3029.

——, and F. Paparella, 2001: Excitation of basin modes by ocean–atmosphere coupling. *Geophys. Res. Lett.,* **28,** 2437–2440.

——, and F. Primeau, 2001: Dissipative selection of low-frequency modes in a reduced-gravity basin. *J. Phys. Oceanogr.,* **31,** 127–137.

——, and P. Otheguy, 2003: Oceanic teleconnections: Remote response to decadal wind forcing. *J. Phys. Oceanogr.,* **33,** 1604–1617.

Dong, B.-W., and R. T. Sutton, 2001: The dominant mechanisms of variability in Atlantic Ocean heat transport in a coupled ocean–atmosphere GCM. *Geophys. Res. Lett.,* **28,** 2445–2448.

——, and ——, 2002: Adjustment of the coupled ocean–atmosphere system to a sudden change in the thermohaline circulation. *Geophys. Res. Lett.,* **29,** 1728.

Döscher, R., C. W. Böning, and P. Herrmann, 1994: Response of circulation and heat transport in the North Atlantic to changes in thermohaline forcing in northern latitudes: A model study. *J. Phys. Oceanogr.,* **24,** 2306–2320.

Eden, C., and T. Jung, 2001: North Atlantic interdecadal variability: Oceanic response to the North Atlantic Oscillation (1865–1997). *J. Climate,* **14,** 676–691.

——, and J. Willebrand, 2001: Mechanism of interannual to decadal variability of the North Atlantic circulation. *J. Climate,* **14,** 2266–2280.

Gerdes, R., and C. Köberle, 1995: On the influence of DSOW in a numerical model of the North Atlantic general circulation. *J. Phys. Oceanogr.,* **25,** 2624–2642.

Goodman, P. J., 2001: Thermohaline adjustment and advection in an OGCM. *J. Phys. Oceanogr.,* **31,** 1477–1497.

Greatbatch, R. J., and K. A. Peterson, 1996: Interdecadal variability and oceanic thermohaline adjustment. *J. Geophys. Res.,* **101,** 20 467–20 482.

——, A. F. Fanning, A. D. Goulding, and S. Levitus, 1991: A diagnosis of interpental circulation changes in the North Atlantic. *J. Geophys. Res.,* **96,** 22 009–22 023.

Häkkinen, S., 2001: Variability in sea surface height: A quantitative measure for the meridional overturning in the North Atlantic. *J. Geophys. Res.,* **106,** 13 837–13 848.

Hallberg, R. H., 1997: Localized coupling between surface and bottom-intensified flow over topography. *J. Phys. Oceanogr.,* **27,** 977–998.

Houghton, J. T., L. G. Meira Filho, B. A. Callender, N. Harris, A. Kattenberg, and K. Maskell, Eds., 2001: *Climate Change 2001: The Scientific Basis*. Cambridge University Press, 944 pp.

Hsieh, W. W., M. K. Davey, and R. C. Wajsowicz, 1983: The free Kelvin wave in finite-difference numerical models. *J. Phys. Oceanogr.,* **13,** 1383–1397.

Huang, R. X., M. A. Cane, N. Naik, and P. Goodman, 2000: Global adjustment of the thermocline in response to deepwater formation. *Geophys. Res. Lett.,* **27,** 759–762.

Huthnance, J. M., 1978: On coastal trapped waves: Analysis and numerical calculation by inverse iteration. *J. Phys. Oceanogr.,* **8,** 74–92.

Johnson, H. L., and D. P. Marshall, 2002a: A theory for the surface Atlantic response to thermohaline variability. *J. Phys. Oceanogr.,* **32,** 1121–1132.

——, and ——, 2002b: Localization of abrupt change in the North Atlantic thermohaline circulation. *Geophys. Res. Lett.,* 1083, **29,** doi:10.1029/2001GL014140.

Karcher, M. J., 1997: Dynamic impact of oscillating sources on the North Atlantic deep circulation: A process study. *J. Geophys. Res.,* **102,** 10 339–10 352.

——, and A. Lippert, 1994: Spin-up and breakdown of source-driven deep North Atlantic flow over realistic bottom topography. *J. Geophys. Res.,* **99,** 12 357–12 373.

Kawase, M., 1987: Establishment of deep ocean circulation driven by deep-water production. *J. Phys. Oceanogr.,* **17,** 2294–2317.

Killworth, P., and J. R. Blundell, 2001: Large-scale propagating disturbances: Approximation by vertical normal modes. *J. Phys. Oceanogr.,* **31,** 2852–2870.

LaCasce, J. H., 2000: Baroclinic Rossby waves in a square basin. *J. Phys. Oceanogr.,* **30,** 3161–3178.

Liu, Z., 1993: Thermocline variability forced by varying Ekman pumping. Part II: Annual and decadal Ekman pumping. *J. Phys. Oceanogr.,* **23,** 2523–2540.

——, 1999: Planetary wave modes in the thermocline: Non-Doppler-shift mode, advective mode and Green mode. *Quart. J. Roy. Meteor. Soc.,* **125,** 1315–1339.

——, 2002: How long is the memory of tropical ocean dynamics? *J. Climate,* **15,** 3518–3522.

——, and J. Pedlosky, 1994: Thermocline forced by annual and decadal surface temperature variation. *J. Phys. Oceanogr.,* **24,** 587–608.

——, L. X. Wu, and E. Bayler, 1999: Rossby wave–coastal Kelvin wave interaction in the extratropics. Part I: Low-frequency adjustment in a closed basin. *J. Phys. Oceanogr.,* **29,** 2382–2404.

Manabe, S., and R. J. Stouffer, 1994: Multiple-century response of a coupled ocean–atmosphere model to an increase of atmospheric carbon dioxide. *J. Climate,* **7,** 5–23.

Marotzke, J., and J. Willebrand, 1991: Multiple equilibria of the global thermohaline circulation. *J. Phys. Oceanogr.,* **21,** 1372–1385.

——, and B. A. Klinger, 2000: The dynamics of equatorially asymmetric thermohaline circulations. *J. Phys. Oceanogr.,* **30,** 955–970.

Munk, W., 1966: Abyssal recipes. *Deep-Sea Res.,* **13,** 707–730.

Primeau, F., 2002: Long Rossby wave basin-crossing time and the resonance of low-frequency basin modes. *J. Phys. Oceanogr.,* **32,** 2652–2665.

Stommel, H. M., 1961: Thermohaline convection with two stable regimes of flow. *Tellus,* **13,** 224–230.

——, and A. B. Arons, 1960: On the abyssal circulation of the World Ocean. Part II: Idealized model of the circulation pattern and amplitude in oceanic basins. *Deep-Sea Res.,* **6,** 217–233.

Wajsowicz, R. C., 1986: Adjustment of the ocean under buoyance forces. Part II: The role of planetary waves. *J. Phys. Oceanogr.,* **16,** 2115–2136.

——, and A. E. Gill, 1986: Adjustment of the ocean under buoyancy forces. Part I: The role of Kelvin waves. *J. Phys. Oceanogr.,* **16,** 2097–2114.

Winton, M., 1996: The role of horizontal boundaries in parameter sensitivity and decadal-scale variations in coarse-resolution ocean general circulation models. *J. Phys. Oceanogr.,* **26,** 289–304.

Yang, J., 1999: A linkage between decadal climate variations in the Labrador Sea and the tropical Atlantic Ocean. *Geophys. Res. Lett.,* **26,** 1023–1026.